On the Bluish Appearance of Veins

by

Spencer R. Van Leeuwen

A thesis
presented to the University of Waterloo
in fulfillment of the
thesis requirement for the degree of
Master of Mathematics
in
Computer Science

Waterloo, Ontario, Canada, 2018

I hereby declare that I am the sole author of this thesis. This is a true copy of the thesis, including any required final revisions, as accepted by my examiners.

I understand that my thesis may be made electronically available to the public.

Abstract

The bluish appearance of veins located immediately beneath the skin has long been a topic of interest for biomedical optics researchers. Despite this interest, a thorough identification of the specific optical processes responsible for this phenomenon remains to be achieved. In this paper, we employ controlled *in silico* experiments to address this enduring open problem. Our experiments, which are supported by measured data available in the scientific literature, are performed using first-principles models of light interaction with human skin and blood. Using this investigation approach, we quantitatively demonstrate that Rayleigh scattering caused by collagen fibrils present in the papillary dermis, a sublayer of the skin, can play a pivotal role in the bluish appearance of veins as suggested by previous works in this area. Moreover, taking colour perception aspects also into account, we systematically assess the effects of variations in fibril radius and papillary dermis thickness on the coloration of veins under different illuminants. Notably, this assessment indicates that Rayleigh scattering elicited by reticulin fibrils, another type of fibril found in the papillary dermis, is unlikely to significantly contribute to the bluish appearance of veins. By strengthening the current understanding about light attenuation mechanisms affecting the appearance of skin and blood, our investigation contributes for the development of more effective technologies aimed at the noninvasive measurement of the physiological properties of these tissues.

Acknowledgements

First and foremost, I would like to thank my supervisor, Gladimir V. G. Baranoski, for all of his support in the development of this thesis. I would also like to thank my thesis committee, Justin Wan and Paulo Alencar, for their participation in my defence. Finally, I would like to thank the other members of the Natural Phenomena Simulation Group, past and present, for their support.

Dedication

This thesis is dedicated to:

My Mom — *Vivianne*

My Sister — *Jessica*

and

My Best Friend — *Ricky*

Table of Contents

List of Tables

List of Figures

Chapter 1

Introduction

Complex optical processes can often lead to counter-intuitive material appearances. Such is the case for the appearance of veins located immediately beneath the skin (Figure 1.1), usually referred to as subcutaneous veins. While skin and venous blood normally do not appear blue in isolation, their combined spectral responses can result in what a human observer may perceive as a bluish appearance.

One light attenuation process known to elicit blue colour in nature is Rayleigh scattering [104, 105]. This type of scattering, caused by structures smaller in magnitude than the wavelength of the affected light, has a stronger effect at the blue end of the visible spectrum. In an early investigation of skin optical properties, it was suggested by Edwards and Duntley [39] that Rayleigh scattering occurring in the epidermis[1] might be responsible for the bluish appearance of veins. However, Anderson and Parrish [6] observed that since the ratio of diffuse transmittance to direct transmittance in the stratum corneum[2] and epidermis is characterized by a weak wavelength dependence, there is not a significant amount of Rayleigh scattering in these tissues. Alternatively, they suggested that a form of scattering characterized by a stronger wavelength dependence could be found in the dermis[3]. It is worth noting that Findlay [40] made a similar observation, although he instead referred to scattering in the dermis as the reflection of light by dermal collagen fibers[4].

[1] A skin layer characterized by the presence of melanin (Section 2.1).

[2] The outermost skin layer (Section 2.1).

[3] A skin layer characterized by the presence of blood (Section 2.1).

[4] An illustration depicting collagen fibers in the dermis and the fibrils composing them is presented in Figure 2.2. These fibers provide a major contribution to the structure of the dermis [33] (Section 2.1).

Figure 1.1: Photograph illustrating the distinct contrast of skin appearance caused by subcutaneous veins.

Oettlé [80] speculated that some form of wavelength-dependent scattering might be caused by fibrils[5] composing the microstructure of collagen fibers found in the dermal tissues of mammals. He also suggested that an irregularity in size and a lack of parallelism of these collagen fibrils, as can be found in the human dermis [8], would not allow for optical interference[6]. Saidi *et al.* [98] suggested that the scattering in the dermal tissues could have a contribution from Mie scattering caused by collagen fibers and from Rayleigh scattering caused by smaller tissue structures. Subsequently, Jacques [50] also speculated that Rayleigh scattering caused by collagen fibrils could explain the good agreement between his mathematical formulation for scattering in the human dermis and measured data.

Cotton and Claridge [30] stated that the conditions for Rayleigh scattering occurring in the papillary dermis would be met with collagen fibers having a diameter of one order of magnitude smaller than the incident light. Electron microscope measurements performed by Arao et al. [8], however, show that the collagen fibrils, instead of the fibers, have a diameter with this order of magnitude.

The most comprehensive investigation of the bluish appearance of veins to date, presented by Kienle *et al.* [54], suggested that it results from several factors. According with their analysis, blue light does not penetrate as deeply into the skin as red light. Consequently, although blood absorbs blue light more strongly than red, less of the blue light

[5] small fibers

[6] The term interference refers to the phenomenon that waves, under certain conditions, intensify or weaken each other [13, 70]. Interference between electromagnetic (light) waves, caused by a material's nanostructure, is known to elicit several distinct colorations in nature [106].

reaches the vein. They suggested that this process, combined with colour perception aspects, provides an explanation for the bluish appearance of veins. It is important to take into account, however, the distinct levels of abstraction employed to characterize the target materials, notably human skin, in their investigation. For example, in their *in silico* experiments involving Monte Carlo simulations, skin was represented by a single homogeneous medium. Kienle *et al.* [54] stated themselves that a multilayer model of human skin should be used for the complete modelling of their *in vivo* measurements. Furthermore, in their *in vitro* experiments, considering five distinct wavelengths and a single illuminant, they employed a phantom medium (a fat emulsion) whose absorptive properties differ markedly from human skin. These experimental constraints might have precluded Kienle *et al.* [54] from identifying specific optical processes resulting from the attenuation of light by heterogeneous media (e.g., Rayleigh scattering), or the location of these processes, in the skin.

The reproduction of the bluish appearance of subcutaneous veins has also been briefly addressed in a computer graphics work by Donner *et al.* [38]. However, their biophysically-inspired approach was intended to visually approximate the appearance of skin rather than to accurately simulate the optical processes occurring within the cutaneous tissues. For instance, they considered the dermis to be semi-infinitely thick, which was justified by their previous claim [37] that an insignificant amount of light reaches the subcutaneous tissues. However, if this claim was physiologically plausible, then subcutaneous veins would not be visible through the skin. To accommodate this modelling decision, they incorrectly placed subcutaneous veins in the junction between the epidermis and dermis, where they were represented as a highly concentrated layer of hemoglobin[7]. They also employed a scattering coefficient formula for *in vitro* human skin [18] to model scattering in the dermis, and considered twice the amount given by this formula to represent the scattering occurring in the epidermis. Since this formula was fitted to data describing the bulk scattering properties of *in vitro* human skin, doubling its predictions has no apparent biophysical meaning. In short, although Donner *et al.* [38] were able to generate images that approximate the bluish appearance of subcutaneous veins, their work lacks the biophysical correctness required for the elucidation of this phenomenon.

[7] A blood-borne pigment primarily responsible for the absorptive behaviour of blood (Section 2.1).

(a)

(b)

Figure 1.2: Photographs demonstrating characteristic hues of cyanotic skin on the (a) hands and (b) feet. Each subfigure presents a cyanotic specimen on the left and a healthy specimen on the right. Photographs ((a)-left and (b)) were provided courtesy of James Heilman, MD.

Recently, the suggestion of Rayleigh scattering being elicited by collagen fibrils [30, 50, 80, 98] was taken into account by Baranoski *et al.* [15] during an *in silico* investigation of the the bluish or purple appearance associated with peripheral cyanosis. More specifically, they used measured radius values for collagen fibrils present in the papillary dermis, obtained by Arao *et al.* [8], to demonstrate that it is necessary to consider Rayleigh scattering in order to elicit the characteristic hues of cyanotic skin (Figure 1.2).

In this work, whose preliminary findings have been presented elsewhere [115], we use a similar approach to show that Rayleigh scattering caused by collagen fibrils present in the papillary dermis can play a pivotal role in the bluish appearance of veins. In our investiga-

tion, we employ *in silico* experiments performed using first-principles models of light interaction with human skin and blood. These models, known as HyLIoS [29] (*Hy*perspectral *L*ight *I*mpingement *o*n *S*kin) and CLBlood [116, 124] (*C*ell-Based *L*ight Interaction Model for Human *Blood*), respectively, account for all significant light-attenuating materials in the skin and blood. The use of an *in silico* framework allowed for highly controlled and reproducible experiments considering detailed specimen characterizations. It also made it possible to disable Rayleigh scattering in the papillary dermis to assess its effect on the appearance of veins. To the best of our knowledge, the technology required to disable light scattering within a thin skin layer, like the papillary dermis, under *in situ* conditions is not available. Assuming that one could attempt to perform such a procedure under *in vitro* conditions, the processes required to extract and prepare a skin sample would alter its optical properties [65].

It is worth remarking that the word "bluish" is used in scientific literature to describe skin tones that appear subjectively blue. As such, bluish skin tones, such as those caused by veins located immediately beneath the skin, may appear closer to grey than blue. Accordingly, the research findings presented in this work have a visual component to allow for a qualitative assessment of appearance.

In addition to addressing a ubiquitous open problem, this work has interesting practical implications. For example, the findings in this work may lead to the development of improved devices for non-invasive measurements of the spectral properties of the skin and subcutaneous veins. Additionally, the biophysically-based framework presented in Section 3 contributes to the state-of-the-art for predictively simulating the appearance of skin with a subcutaneous vein, which has potential applications in computer graphics. A more in-depth discussion of the contributions of this work can be found in Section 7.

The remainder of this thesis is organized as follows. In Chapter 2, we discuss light attenuation processes that occur within the skin and blood in the visible domain (400–700 nm). This will serve as a foundation for our investigation and discussion. Next, in Chapter 3, we concisely describe the models employed in this investigation and how they were employed to simulate the optical properties of a skin specimen with a vein immediately beneath it. We then outline our *in silico* experimental setup in Chapter 4, present our findings in Chapter 5, and discuss their implications in Chapter 6. In Chapter 7, we conclude the thesis and provide potential directions for future work.

Chapter 2

Biophysical Background

In this chapter, we describe the tissues relevant to the appearance of veins. For each tissue, we outline the constituent materials that contribute significantly to the attenuation of light in the visible domain. Measured absorption spectra for all pigments discussed in this chapter are presented in Figure 2.1. We also discuss the role of the detour and sieve effects in the optical properties of skin and blood.

2.1 Skin

The cutaneous tissues are usually divided into three distinct layers, namely the stratum corneum, epidermis and dermis, from the outermost to the innermost [7, 33]. From outermost to innermost, they are the stratum corneum, epidermis and dermis [121]. The epidermis can be further subdivided into four sublayers: stratum lucidum, stratum granulosum, stratum spinosum and stratum basale. The dermis, in turn, can be subdivided into two sublayers: papillary dermis and reticular dermis. It is worth noting that the stratum lucidum is a clear layer found only in thick skin regions such as the palms and soles [33]. For this reason, it is usually not considered in skin optics investigations.

The absorption of light traversing the stratum corneum and epidermis is dominated by melanin with a minor contribution from beta-carotene (Figure 2.1(b)) [7]. Melanin is synthesized and preferentially concentrated in the stratum basale [33]. Melanin can be classified as either brown-black eumelanin or yellow-red pheomelanin (Figure 2.1(a)), the former of which has a significantly higher concentration in skin. Melanin can be dispersed throughout the epidermis in colloidal form or clustered within organelles called melanosomes [84].

In the skin, light is mostly scattered by heterogeneous structures such as cells, organelles and fibers [7]. Goniometric measured data [25] and empirical observations available in the literature [6, 114] indicate that both the stratum corneum and epidermis are characterized by a strong forward scattering behaviour exhibiting slight variations with wavelength. Scattering in the epidermis is dominated by melanosomes [58] which can be described as particles with the shape of a prolate spheroid [81] and a melanin concentration of 17.9% to 72.4% [58]. In lightly pigmented specimens, melanosomes can occur in groups surrounded by a transparent membrane, known as melanosome complexes [81, 109]. In addition to empirical observations indicating that a significant amount of Rayleigh scattering does not occur in the stratum corneum and epidermis [6,40], it has been shown that the consideration of scattering caused by melanosomes and melanosome complexes is sufficient to predictively model the scattering behaviour of the stratum corneum and epidermis in the blue region of the light spectrum [29].

The outermost dermal layer, the papillary dermis, is composed of loosely packed collagen and reticulin fibers which, in turn, are composed of smaller-sized fibrils (Figure 2.2). Since these fibrils are smaller in magnitude than the wavelength of light within the visible spectrum, any scattering caused by these structures would likely follow the Rayleigh scattering theory [104, 105]. The innermost dermal layer, the reticular dermis, is composed of dense irregular connective tissue formed by densely packed collagenous fibers arranged in a tight interwoven pattern [33]. A network of blood vessels also runs throughout the dermis with wider vessels in the reticular dermis. Blood-borne pigments within these vessels (Figure 2.1(b)–(d)) dominate the dermis's absorptive behaviour in the visible domain [53]. Furthermore, the diffusion of red light traversing the reticular dermis [52] results from scattering by the dense collagen fibers (following a Mie scattering behaviour [50]) and the wider blood vessels. Since this scattering is significant enough to diffuse the light, it would likely dominate any Rayleigh scattering that may occur in the reticular dermis.

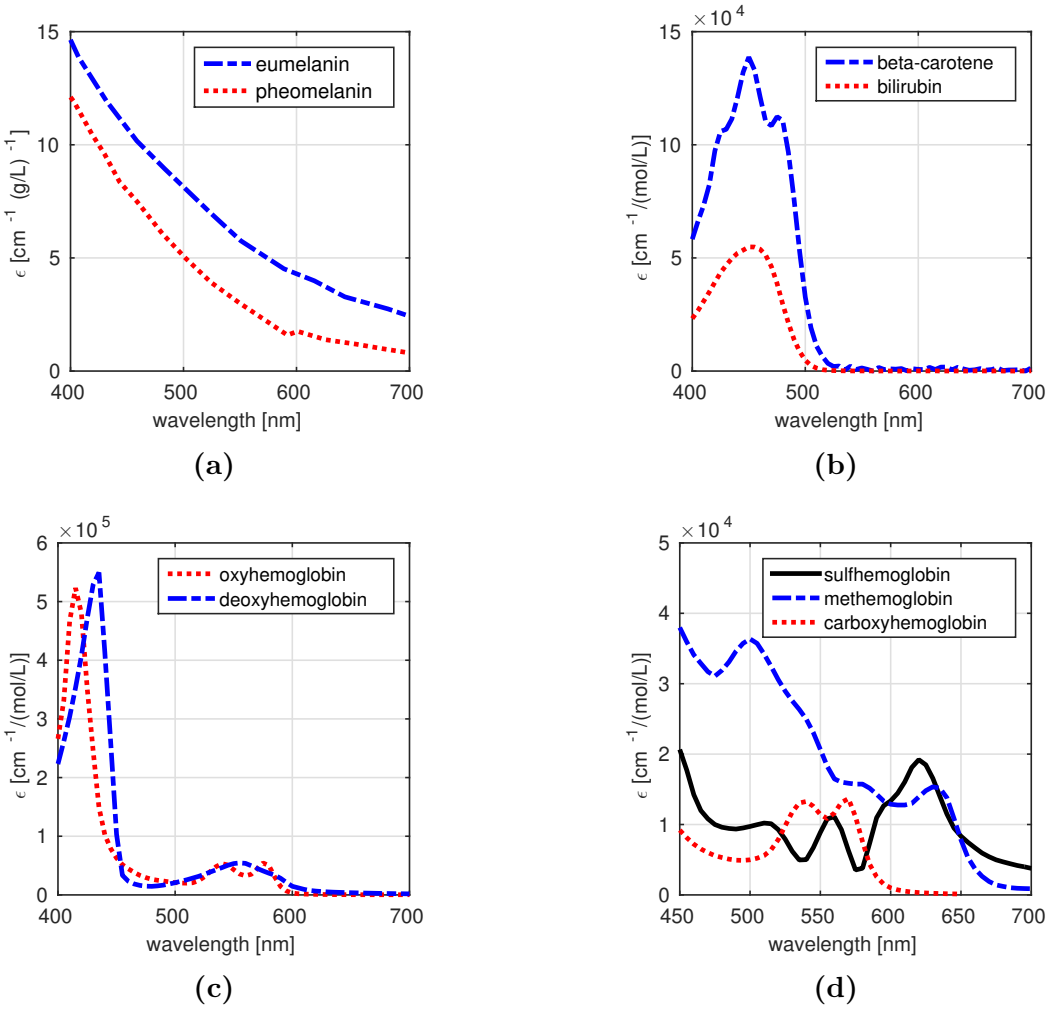

Figure 2.1: Absorption data for skin and blood pigments with a significant impact on light attenuation in the visible domain. (a) Extinction coefficient curves for the melanins considered in this investigation [51]. (b) Molar extinction coefficient curves for beta-carotene and bilirubin [89]. (c) Molar extinction coefficient curves for the functional hemoglobins [88]. (d) Molar extinction coefficient curves for the dysfunctional hemoglobins [91, 102, 123].

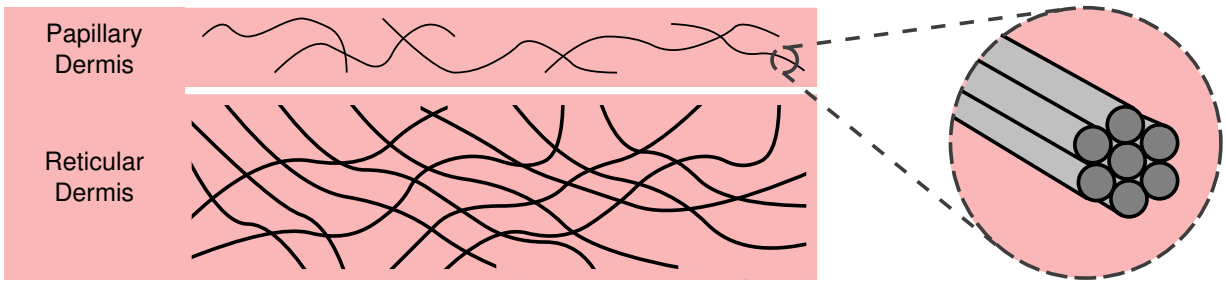

Figure 2.2: An illustration depicting the loosely packed collagen fibers in the papillary dermis and the thicker, densely packed collagen fibers in the reticular dermis. On the right, we can observe that the fibers are composed of smaller-sized collagen fibrils. Note that for simplicity, our illustration does not capture the fact that collagen fibrils (when examined by an electron microscope [8]) are irregular in size and are not parallel.

2.2 Blood

This highly specialized connective tissue is composed of plasma and various types of cells, known as formed elements [69]. Red blood cells, or erythrocytes, make up 99% of the formed elements in the blood and each one consists of a thin membrane encapsulating a hemoglobin solution. The attenuation of light by red blood cells exceeds that of other blood components by 2–3 orders of magnitude [69]. The absorption of light by red blood cells in the visible domain is primarily attributed to the hemoglobins (Figure 2.1(c) and (d)) and the scattering of light is determined by their shape and orientation [55].

The orientation of red blood cells in a flowing blood sample can change depending on its shear rate (*i.e.*, the velocity gradient in the direction normal to the flow) [63]. At low, intermediate and high shear rates, the red blood cells are predominantly randomly oriented, rolling or aligned with the direction of the flow, respectively [63]. When the volume fraction of blood occupied by formed elements, known as hematocrit, is above 40%, the alignment of the red blood cells becomes more pronounced [63].

2.3 Hypodermis

This subcutaneous tissue is located immediately beneath the skin except for certain regions of the body (e.g., eyelids) in which it is not present [33]. It consists mostly of white fat cells that contain lipidic vesicles [2]. The size of these spherical droplets of lipids are larger

than that of typical scatterers [18]. This may explain the strong backscattering behaviour of this adipose tissue, comparable with the dermis's behaviour and much stronger than the behaviour of other types of tissues like cartilages and muscles, which was verified in actual experiments [100]. The most abundant light absorbers found in the hypodermis, namely water (10-30% [2] and lipids (70-90% [2]), have a negligible impact in the visible domain [5, 78, 82, 86]. Due the strong absorptive properties of cutaneous melanin in the blue region of the light spectrum, only a negligible amount of light in this region is likely to reach the hypodermis [7]. Experiments by Dinish *et al.* [35] show that 90 to 95% of light in the red and green regions of the light spectrum are reflected by white adipose tissue. Accordingly, the majority of the visible light that reaches the hypodermis is likely to be scattered by the droplets of lipids and remitted into the reticular dermis [121].

2.4 Vein Wall

Vein walls are composed of elastin, collagen and muscle tissue [108]. The absorption of visible light within a vein wall is dominated by hemoglobin in the muscle tissue (Figure 2.1(c) and (d)) [19]. It is also possible that light traversing a vein wall may be scattered by its heterogeneous structures.

2.5 Detour and Sieve Effects

Skin and blood are both turbid mediums characterized by their heterogeneously-distributed, pigment-containing structures. Notably, the attenuating properties of melanosomes and red blood cells play an important role in the optical processes of skin and blood, respectively. When light traverses a turbid medium, scattering by these structures can increase its optical pathlength, which results in an increased probability of absorption. Conversely, light may not encounter any pigment-containing structure, which results in a decreased probability of absorption. These phenomena are respectively known as the detour effect [26] and the sieve effect [61]. The combined contribution of these effects to the overall absorptive behaviour of a turbid medium depends on the properties and distribution of the medium's pigment-containing structures.

Chapter 3

Experimental Framework

In this chapter, we describe provide a brief background on the HyLIoS [29] and CLBlood [116, 124] models and describe how they are employed to represent the skin specimens considered in our experiments. In particular, we discuss the representation of skin specimens with and without a vein immediately beneath the skin (i.e., with and without a subcutaneous vein).

3.1 Models Background

In our *in silico* experiments, we use HyLIoS [29] and CLBlood [116, 124] to simulate the interactions of light with skin and flowing venous blood, respectively. Both of these models have been evaluated extensively against measured data in their original publications [29, 124]. CLBlood was also recently updated and re-evaluated [116].

HyLIoS and CLBlood are both first-principles models that employ measured optical properties of constituent materials to control the propagation and attenuation of light within human skin and blood. Although this paper is focused on light in the visible domain, it is worth noting that both models consider all constituent materials with a significant contribution to light attenuation in the ultraviolet, visible and near-infrared domains. Measured optical properties for these constituent materials were obtained from scientific literature and made available online [73, 74]. References to this data can also be found in the models' original publications [29, 124]. Additionally, HyLIoS and CLBlood account for sieve and detour effects by individually distributing melanosomes throughout the epidermis and red blood cells throughout the plasma, respectively. This includes the

grouping of melanosomes within melanosome complexes. As pointed out by Lister *et al.* [65], the size and distribution of these melanin-containing structures have been often overlooked when simulating their effects on skin colour.

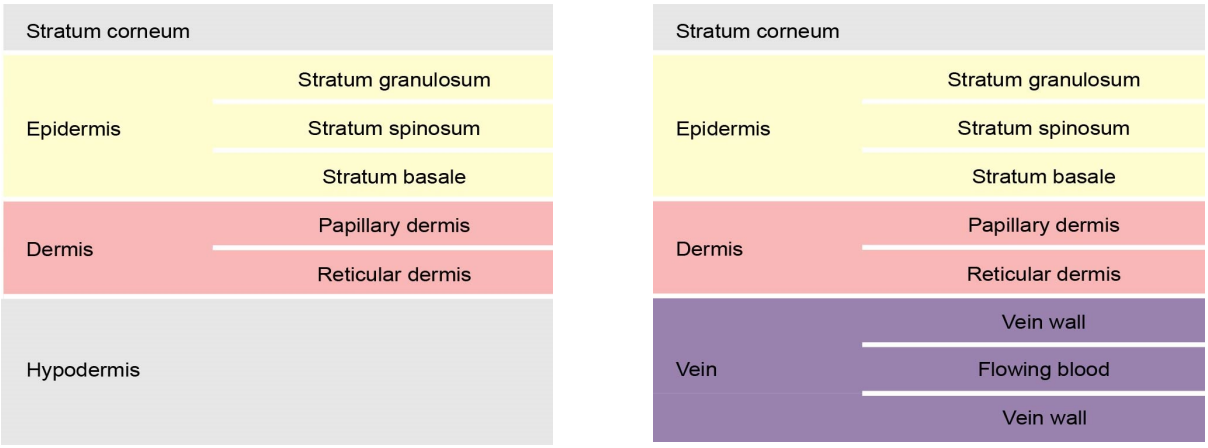

Figure 3.1: Diagrams depicting the layers considered in our experimental framework for skin specimens (a) without a subcutaneous vein and (b) with a subcutaneous vein.

3.2 Skin Specimen without a Subcutaneous Vein

For the skin specimens without a subcutaneous vein, we used the HyLIoS model as described in its original publication [29]. In particular, there is a layer below the reticular dermis that represents the hypodermis (Figure 3.1(a)). We remark, as outlined in Section 2.3, that the amount of light in the blue region reaching this layer is negligible due to the cutaneous pigmentation [7] and most of the light in the green and red regions is reflected back [35]. Thus, by reflecting the visible light that may reach the hypodermis, a strategy also employed by several relevant works on skin colour reproduction (e.g., the interested reader is referred to the works by Cotton and Claridge [30] and by Doi and Tominaga [36]), one can minimize the introduction of undue computational overhead in the simulations without reducing the fidelity of the simulations. Accordingly, we assume that visible light reaching the hypodermis is diffusely reflected back into the reticular dermis. The diffusion distribution in this case accounts for the overall scattering behaviours of both reticular dermis [52] and hypodermis [100] as also outlined earlier (Sections 4.1 and 2.3). The implications of this simulation choice are further discussed in Section 6.5.

3.3 Skin Specimen with a Subcutaneous Vein

For the skin specimens with a subcutaneous vein, the hypodermis layer is replaced by the vein (Figure 3.1(b)). We use a three layer model to represent the vein (Figure 3.1(b)). The first and third layers represent the vein wall and the second layer employs CLBlood to account for flowing venous blood. When light encounters the boundary of a layer, a Fresnel test[1] [7] is performed to determine whether the light is reflected or transmitted.

We do not consider any absorption or scattering of light within the vein wall. In addition, any light that is transmitted below the bottom vein wall layer is discarded. The scientific reasonings behind each of these simulation choices, which were also implemented to avoid undue computational overhead without reducing the fidelity of our simulations, are further discussed in Sections 6.1 and 6.6, respectively.

3.4 Vein Precomputation

Since we know that visible light transmitted by the dermis is diffusely distributed when considering a typical physiological thickness [52], we can assume a uniform distribution for the angle of incidence of all light that encounters the vein. This assumption allows us to precompute the probability that light is reflected by the vein using the representation outlined in Section 3.3. To obtain this probability, we first compute the reflectance of the vein considering polar angles in the range $[0°, 90°)$ at each $5°$ interval and azimuthal angles in the range $[0°, 360°)$ at each $90°$ interval. For each angle of incidence, the reflectance calculations are performed considering 10^5 sample rays per wavelength. Since we assume that the light entering the vein is uniformly distributed, we average the reflectance values across all samples at each wavelength to get the overall probability of light being reflected by the vein. When performing our experiments, we employ this precomputed probability to determine whether a light ray that encounters the vein will be reflected diffusely or discarded (i.e., absorbed or transmitted).

[1] When light moves between media with distinct refractive indices, there is a chance that it will be reflected. The probability of light being reflected can be modelled by the Fresnel coefficient for the interface [7]. This coefficient is a function of the mediums' refractive indices and the angle of incidence of the light. A Fresnel test consists in generating a random number ($\xi \in [0, 1]$) from a uniform distribution and comparing it against the Fresnel coefficient (F) [7]. If $\xi \leq F$ then the given light ray is reflected, otherwise it is transmitted.

Chapter 4

In Silico Experimental Setup

In this chapter, we present the data used in our experimental setup. This includes data relating to measurement procedures and specimen characterizations.

In our experiments, we computed directional-hemispherical reflectance curves for various skin specimens with a virtual spectrophotometer [14] considering a 5° angle of incidence, 10^6 sample rays per wavelength, and a 5 nm spectral resolution. We then used the computed reflectance data to generate textured colour swatches using the method described in Section 4.4.

In each experiment set, we consider skin specimens with and without a subcutaneous vein. The skin specimen characterizations considered in each experiment set are outlined in Section 4.1. We remark that they are based on measured data provided in the scientific literature. In order to evaluate the contribution of Rayleigh scattering to the reflectance and appearance of the specimens, each experiment set includes results that consider Rayleigh scattering as well as results that do not consider it. The method used to disable Rayleigh scattering occurring in the papillary dermis is presented in Section 4.3. The vein-related parameters and quantities considered in all experiments are described in Section 4.2 and the online reproducibility of the results presented in this work is addressed in Section 4.5.

4.1 Experimental Sets

We performed three sets of *in silico* experiments. In Experiment Set #1 (Figures 5.1 and 5.2), we consider a baseline skin specimen characterized by the parameter values presented in Tables 4.1 and 4.2. Accompanying each of these values is a list of references that provide their physiological basis. We remark that the thickness of our skin specimen is within a measured range of thickness for skin on the dorsum of the hand [43].

In Experiment Set #2 (Figure 5.3), we multiply the melanin content and dermal blood content parameters in Table 4.2 by $f_{mel} \in \{1.0, 1.5, 2.0, 2.5\}$ and $f_{bl} \in \{1.0, 1.5, 2.0, 2.5\}$, respectively, to obtain additional skin specimens. For each experiment, the mean epidermal melanin content is in the range 1–3% and dermal blood content is in the range 2-6%, corresponding to the physiological characterization of a lightly pigmented specimen [64]. Our justification for focusing on lightly pigmented specimens in our investigation is provided in Section 6.3.

In Experiment Set #3 (Figures 5.4-5.8), we varied the radius of the fibrils in the papillary dermis and the thickness of the papillary dermis. We considered fibril radius values in the range 20–60 nm and papillary dermis thickness values in the range 0.0025–0.02 cm. These ranges are based on measurements of collagen and reticulin fibril radius [3, 8] as well as reported values for papillary dermis thickness [3, 6, 24, 27].

Table 4.1: HyLIoS parameters employed in the general characterization of all skin specimens considered in this investigation. Note that in the last two rows, the scatterers correspond to the fibrils in the papillary dermis.

HyLIoS Parameters	Values	References
Aspect Ratio of Skin Surface Fold	0.1	[67, 110]
Stratum Corneum Thickness (cm)	0.0004	[1, 85, 90, 92]
Stratum Granulosum Thickness (cm)	0.0033	[93]
Stratum Spinosum Thickness (cm)	0.0033	[93]
Stratum Basale Thickness (cm)	0.0033	[101]
Reticular Dermis Thickness (cm)	0.125	[6, 27]
Stratum Granulosum Melanosome Content (%)	0.0	[58, 64]
Stratum Spinosum Melanosome Content (%)	0.0	[58, 64]
Stratum Basale Melanosome Dimensions ($\mu m \times \mu m$)	0.41×0.17	[81]
Melanosome Eumelanin Concentration (mg/mL)	32.0	[47, 112]
Melanosome Pheomelanin Concentration (mg/mL)	2.0	[47, 112]

Dermal Oxyhemoglobin Fraction (%)	90.0	[79]
Hemoglobin Concentration in Blood (mg/mL)	147.0	[41, 66]
Methemoglobin Concentration in Blood (mg/mL)	1.5	[97]
Carboxyhemoglobin Concentration in Blood (mg/mL)	1.5	[32]
Sulfhemoglobin Concentration in Blood (mg/mL)	0.0	[123]
Blood Bilirubin Concentration (mg/mL)	0.003	[96]
Stratum Corneum Beta-carotene Concentration (mg/mL)	2.1E-4	[62]
Epidermis Beta-carotene Concentration (mg/mL)	2.1E-4	[62]
Blood Beta-carotene Concentration (mg/mL)	7.0E-5	[62]
Stratum Corneum Water Content (%)	35.0	[3, 72]
Epidermis Water Content (%)	60.0	[3, 118]
Papillary Dermis Water Content (%)	75.0	[3, 118]
Reticular Dermis Water Content (%)	75.0	[3, 118]
Stratum Corneum Lipid Content (%)	20.0	[120]
Epidermis Lipid Content (%)	15.1	[3, 28, 103]
Papillary Dermis Lipid Content (%)	17.33	[3, 28, 103]
Reticular Dermis Lipid Content (%)	17.33	[3, 28, 103]
Stratum Corneum Keratin Content (%)	65.0	[44, 45, 101]
Stratum Corneum Urocanic Acid Density (mol/L)	0.01	[125]
Skin DNA Density (mg/mL)	0.185	[3, 42, 117]
Stratum Corneum Refractive Index	1.55	[34, 111]
Epidermis Refractive Index	1.4	[111, 113]
Papillary Dermis Refractive Index	1.39	[52, 111]
Reticular Dermis Refractive Index	1.41	[52, 111]
Melanin Refractive Index	1.7	[17]
Papillary Dermis Scatterers' Refractive Index	1.53	[119]
Papillary Dermis Fraction Occupied by Scatterers (%)	22.0	[50]

Table 4.2: HyLIoS melanin and blood content parameters that are modified to produce different skin specimen characterizations. The presented values correspond to the baseline skin specimen. The melanin parameters* and blood parameters† are multiplied by a factor of f_{mel} and f_{bl}, respectively, to provide the skin specimens in Experiment Set #2.

HyLIoS Parameters	Values	References
Stratum Basale Melanosome Content (%)	1.0 *	[58, 64]
Stratum Granulosum Colloidal Melanin Content (%)	0.5 *	[4, 58, 64, 84]
Stratum Spinosum Colloidal Melanin Content (%)	0.5 *	[4, 58, 64, 84]
Stratum Basale Colloidal Melanin Content (%)	0.5 *	[4, 58, 64, 84]
Papillary Dermis Blood Content (%)	0.2 †	[27, 41, 50, 64]
Reticular Dermis Blood Content (%)	0.2 †	[27, 41, 50, 64]
Radius of Papillary Dermis Scatterers (nm)	40.0	[3, 8]
Papillary Dermis Thickness (cm)	0.02	[3, 6, 24, 27]

4.2 Vein-Related Data

In our precomputation (Section 3.4) of the probability of light being reflected by the vein ($p^r_{vein}(\lambda)$), we considered the blood characterization data presented in Table 4.3. It is worth noting that the thickness of the blood sample, 1270 μm, corresponds to the lumen diameter of a vein on the dorsum of the hand [56].[1]. The refractive index selected for the vein wall is 1.39, which corresponds to a measured value for the vena femoralis[2] [95]. The resulting curve for $p^r_{vein}(\lambda)$ is presented in Figure 4.1.

[1]The opening in the vein through which the blood flows [33].

[2]This vein is also known as the femoral vein and is located in the thigh [33].

Table 4.3: CLBlood parameters employed in the characterization of the blood flowing through the subcutaneous vein.

CLBlood Parameters	Values	References
Hematocrit (%)	45	[10, 71]
Sample Thickness (μm)	1270.0	[56]
Randomly Oriented Cells (%)	10	[57, 63, 83]
Rolling Oriented Cells (%)	60	[57, 63, 83]
Aligned Oriented Cells (%)	30	[57, 63, 83]
Oxyhemoglobin (%)	67.9	[126]
Deoxyhemoglobin (%)	29.1	[126]
Sulfhemoglobin (%)	0	[122]
Methemoglobin (%)	1.5	[46]
Carboxyhemoglobin (%)	1.5	[31]
Mean Cell Hemoglobin Content (g/L)	330.0	[10]

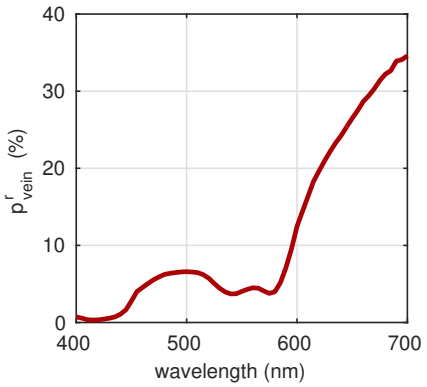

Figure 4.1: The precomputed probability of light being reflected by the subcutaneous vein specimen (p^r_{vein}) employed in our experiments. This curve was computed using the procedure outlined in Section 3.4 considering the blood characterization data presented in Table 4.3.

4.3 Rayleigh Scattering Simulation

Within the HyLIoS' formulation [29], the direction of a light ray traversing the papillary dermis can be perturbed considering the Rayleigh scattering distribution [68]. Ideally, one would like to consider the exact geometric shape of the fibrils and directly simulate the interaction of light with each one of them. However, such an approach would not only represent a challenging project in itself, deserving a publication in its own right like the work of Arifler *et al.* [9] on ocular stroma, but would be also severely constrained by data scarcity. Alternatively, one needs to resort to an approximation and take into account its practical implications.

In the work by Saidi *et al.* [98], the authors employed infinitely long cylinders placed parallel to the skin surface to represent fibers eliciting Mie scattering. Incidentally, their algorithm was based on the work by Bohren and Huffmann [23]. Although a similar approximation could be potentially employed for the scattering elicited by fibrils, a few aspects have to be taken into account when assessing its suitability for the problem at hand.

As pointed out by Bohren [22], scattering by spheres and by infinitely long circular cylinders illuminated normally to their axes are in some ways similar. For example, spherical Bessel functions employed in the formulation of sphere scattering coefficients correspond to cylindrical Bessel functions employed in the formulation of cylinder scattering coefficients. Different from a sphere, however, an infinitely long cylinder cannot be confined within a finite volume, which impacts the way the scattering varies with the radius of the scatterers [22].

Moreover, recall that Rayleigh scattering is dependent on the wavelength of light to the power of -4, which corresponds to the Rayleigh limit of the Mie scattering theory [50, 68], and it is characterized by forward and backward lobes leading to an isotropic behaviour on average [68,98]. As also pointed out by Bohren [22], the use of other type of approximations (e.g., cylinders) in scattering formulations originally proposed considering homogeneous spheres, like the Rayleigh theory which is included in the Mie theory, would be "risky", especially for computing scattering toward the backward direction.

If the fibrils present in the papillary dermis were characterized by a preferred orientation, this might represent an argument in favour of a cylindrical approximation. However, the irregular distribution of collagen fibrils suggested by Oettle [80] was corroborated by the electron microscope images provided by Arao *et al.* [8] showing no preferred orientation for these structures in the papillary dermis.

Hence, representing the scatterers of interest, namely the fibrils, by spheres, albeit

having the shortcomings of any approximation, provides the best fidelity/cost ratio in comparison with other alternatives, like cylinders, since it allows us to avoid undue complexity and the introduction of bias in the simulation of backscattering as indicated by Bohren [22]. For these reasons, we have selected the following formula for the scattering coefficient controlling the probability of Rayleigh scattering events [29, 59, 68]:

$$\mu_s^R(\lambda) = \frac{32\pi^4 r^3 v_f}{\lambda^4} \left(\frac{\eta^2 - 1}{\eta^2 + 1} \right)^2, \tag{4.1}$$

where v_f represents the volume fraction of the papillary dermis occupied by fibrils and r represents the radius of the fibrils. The variable η is the ratio between the refractive index of the fibrils (η_f) and the refractive index of the papillary dermis (η_{pd}). To deactivate Rayleigh scattering, we simply set $\eta_f = \eta_{pd}$ which results in $\mu_s^R = 0$ and, hence, a 0% probability that a Rayleigh scattering event occurs. The values for v_f, η_{pd} and the baseline value for η_f are given in Table 4.1. The baseline value for r is given in Table 4.2.

It is worth noting that the thickness of the papillary dermis (t_{PD}) also indirectly affects how much Rayleigh scattering will occur. This can be explained by the fact that the the probability of light being attenuated while traversing a given layer tends to be higher for thicker layers [87].

4.4 Swatch Generation

Swatches are used in this work to approximate the appearance of a given skin specimen under distinct illumination conditions. To generate the colour of a swatch, the skin specimen's modelled reflectance curve is convolved with the selected illuminant's relative spectral power distribution and the broad spectral response of the human photoreceptors [48] (Appendix C). The last step involves a standard CIE XYZ to sRGB conversion procedure [12] which includes a white balancing calculation considering the selected illuminant.

In our investigation, we considered four standard CIE illuminants, namely D50, D65, A and F2 [48], whose relative spectral power distributions are presented in Figure 4.2. D50 and D65 approximate daylight at different times of day, A corresponds to an incandescent light, and F2 represents a "cool white fluorescent" light typical of an office environment [48]. Since F2 was published independently of the other illuminants, and the employed data was provided in relative units, we decided to increase its intensity in the swatch generation process to get a similar qualitative brightness across the swatches. We selected D65 for the experimental instances in which we considered a single illuminant (Figures 5.3 and 5.8).

After computing the colour of a swatch, we apply a greyscale texture to it in order to make the synthetic depiction of skin more realistic. In Figures 5.3 and 5.8, each swatch depicts a zoomed-out view of skin with a vein running beneath it. Note that in these swatches, not only the skin area above the vein, but also the area around it are rendered with their corresponding colours. This allows us to implicitly account for colour perception phenomena related to the retinex theory [60]. This theory proposes that the spectral remission from a given area alone does not determine its colour, i.e., one must also consider the remission from surrounding areas. According with Kienle *et al.* [54], retinex theory should be taken into account when assessing the perception of a vein's appearance as seen by a human observer.

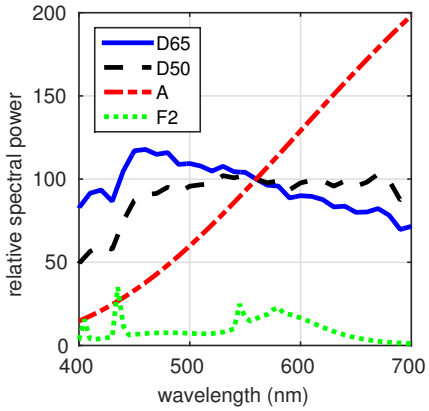

Figure 4.2: Relative spectral power distribution of each CIE standard illuminant [48] employed in the swatch generation process described in Section 4.4.

4.5 Online Reproducibility

The experiments in this work can be reproduced with our online versions of HyLIoS [77] and CLBlood [76] which are deployed using a custom model distribution system [75]. This system allows a user to perform their own experiments with a specified skin specimen characterization and experimental setup. The online version of HyLIoS has been updated to facilitate the reproduction of the reflectance of a skin specimen with a subcutaneous vein considering a chosen venous blood oxygenation. Additionally, we have made it possible to reproduce the reflectance of an isolated vein from a single angle of incidence using our online version of CLBlood [76].

Chapter 5

Experimental Results

In this chapter, we present the results of the experiments described in Chapter 4. To accommodate colour-blind readers, Appendix B provides RGB triplet values for all generated colour swatches presented in this chapter.

5.1 Experiment Set #1

For our first set of experimental results, we explore the effect of disabling Rayleigh scattering in the papillary dermis on the reflectance and appearance of the baseline skin specimen with and without a subcutaneous vein. First, we examine the reflectance results which are presented in Figure 5.1. When Rayleigh scattering is enabled (Figure 5.1(a)), there is a smaller difference between the reflectance curves of the skin specimens with and without a subcutaneous vein in the short (blue) wavelength range. In particular, the difference between the two curves is negligible in the region near 400 nm. Given the near zero probability of light being reflected by the vein in this region (Figure 4.1), the light must have been scattered out of the skin before it could reach the vein.

Since this behaviour could potentially be attributed to Rayleigh scattering, let us examine the reflectance results for the experiments without Rayleigh scattering presented in Figure 5.1(b). We can observe that disabling Rayleigh scattering reduces the reflectance significantly for both specimens in the region near 400 nm. Furthermore, the amount of reflected light in this region is lower for the skin specimen with a subcutaneous vein. This indicates that the absence of Rayleigh scattering allowed more light to reach and, hence, be absorbed by the vein.

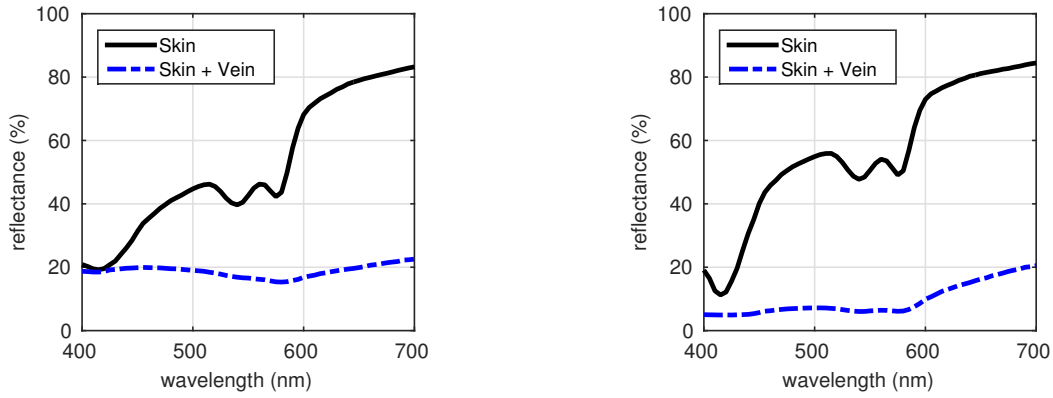

Figure 5.1: Modelled reflectance curves obtained for the baseline skin specimen with and without a subcutaneous vein. (a) With Rayleigh scattering. (b) Without Rayleigh scattering.

Now, let us examine Figure 5.2 to see how these differences in reflectance translate to appearance. The appearance swatches presented in Figure 5.2(a) were generated using the reflectance data from the experiments with Rayleigh scattering (Figure 5.1(a)) and considering several illuminants. The colours depicted in these swatches generally match our expectations for the appearance of skin with and without a subcutaneous vein. Accordingly, the RGB (Red, Green, Blue) colour triplets used to generate these swatches, presented in Table 5.1(a), quantitatively show that the colours elicited by the skin specimen with a subcutaneous vein have a blue component that exceeds in magnitude its red and green counterparts (for all considered illuminants). Conversely, the swatches presented in Figure 5.2(b), computed considering the reflectance data from the experiments without Rayleigh scattering (Figure 5.1(b)), present a brownish-red appearance for the skin specimen with a subcutaneous vein. For this specimen, we can also observe that the red component of the RGB triplets presented in Table 5.1(b) exceeds in magnitude its green and blue counterparts.

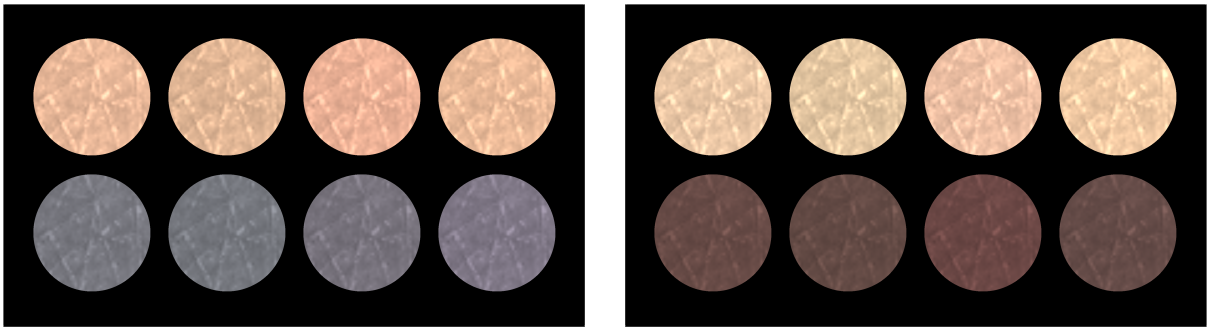

(a) **(b)**

Figure 5.2: Generated swatches depicting the effect of Rayleigh scattering in the papillary dermis on the appearance of the baseline skin specimen without (top) and with (bottom) a subcutaneous vein. From left to right, the swatches in each subfigure were generated considering CIE standard illuminants D50, D65, A and F2. (a) With Rayleigh scattering. (b) Without Rayleigh scattering. The computed RGB triplet values used to generate the swatches in this figure are presented in Tables 5.1 and B.1 (Appendix B).

Table 5.1: The RGB (Red, Green, Blue) triplets employed in the generation of the swatches presented in Figure 5.2. Each RGB triplet is computed using the modelled reflectance data for the baseline skin specimen with and without a subcutaneous vein considering CIE standard illuminants D50, D65, A and F2, as described in Appendix C. (a) With Rayleigh scattering. (b) Without Rayleigh scattering.

	D50	D65	A	F2
Skin	(242,191,159)	(234,189,155)	(256,185,156)	(245,194,159)
Skin + Vein	(124,125,133)	(121,124,131)	(124,119,129)	(132,124,139)

(a)

	D50	D65	A	F2
Skin	(245,208,173)	(237,206,168)	(248,200,171)	(251,210,170)
Skin + Vein	(108,78,73)	(103,77,72)	(111,74,72)	(105,79,75)

(b)

5.2 Experiment Set #2

Swatches belonging to our second set of experimental results are presented in Figure 5.3. They show that the role of Rayleigh scattering in the appearance of a skin specimen with a subcutaneous vein is consistent when considering different levels of melanin content and dermal blood content.

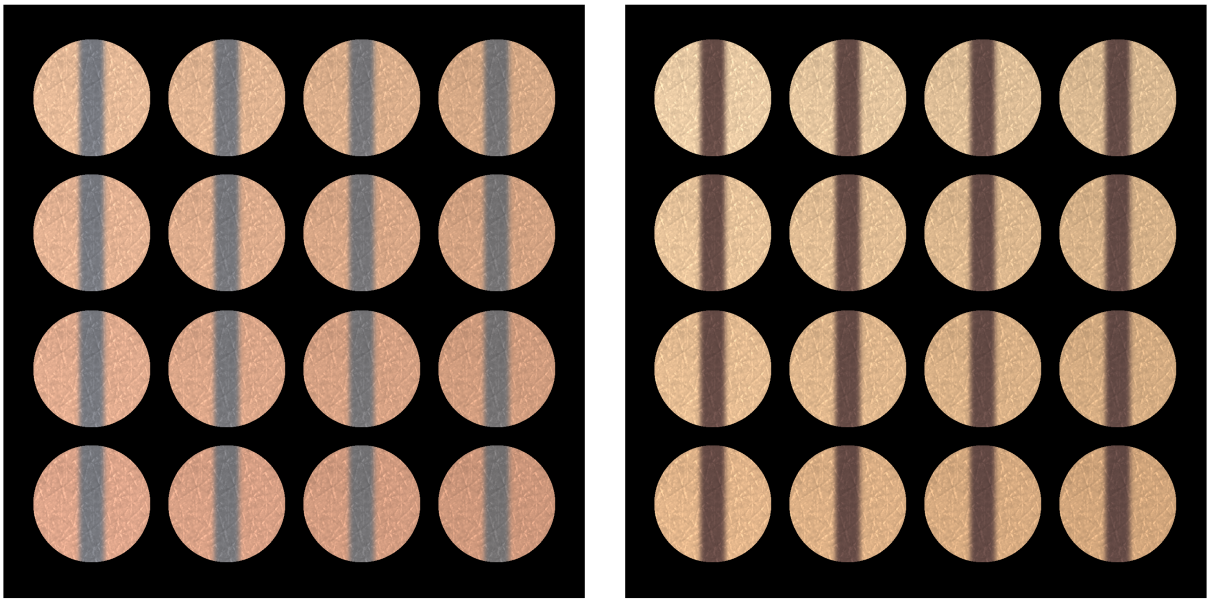

(a) **(b)**

Figure 5.3: Generated swatches depicting several skin specimens with a subcutaneous vein running beneath them considering the CIE standard illuminant D65. Distinct skin specimens were obtained by multiplying melanin and blood content (Table 4.2) by f_{mel} and f_{bl}, respectively. Left to right: $f_{mel} = 1.0, 1.5, 2.0, 2.5$. Top to bottom: $f_{bl} = 1.0, 1.5, 2.0, 2.5$. (a) With Rayleigh scattering. (b) Without Rayleigh scattering. Note that the baseline skin specimen corresponds to $f_{mel} = 1.0$ and $f_{bl} = 1.0$. The computed RGB triplet values used to generate the swatches in this figure are presented in Tables B.2 and B.3 (Appendix B).

5.3 Experiment Set #3

Since our results indicate that Rayleigh scattering in the papillary dermis contributes to the appearance of veins, let us examine the effect of varying the values of parameters that have an impact on the amount of Rayleigh scattering occurring in the papillary dermis.

The results presented in Figure 5.4 show the effect of varying the radius of the fibrils in the papillary dermis on the reflectance of skin specimens with and without a subcutaneous vein. For the skin specimens without a subcutaneous vein (Figure 5.4(a)), we can see that a higher fibril radius corresponds to a lower reflectance, except in the region near 400 nm. For the skin specimen with a subcutaneous vein (Figure 5.4(b)), a higher fibril radius corresponds to a higher reflectance across the visible spectrum. We can also observe in Figure 5.4(b) that the difference between the reflectance of the baseline skin specimen ($r = 40$ nm) and the reflectance of a skin specimen with a higher fibril radius ($r = 50$ and 60 nm) is the greatest in the middle of the visible spectrum, a region corresponding to what a human observer would perceive as green colour. In both subfigures (Figure 5.4(a) and (b)), we can see that skin specimens with a small fibril radius ($r = 20$ and 30 nm) have reflectance curves that resemble the reflectance curves presented in Figure 5.1(b), which correspond to the experiments considering the baseline skin specimen without any Rayleigh scattering.

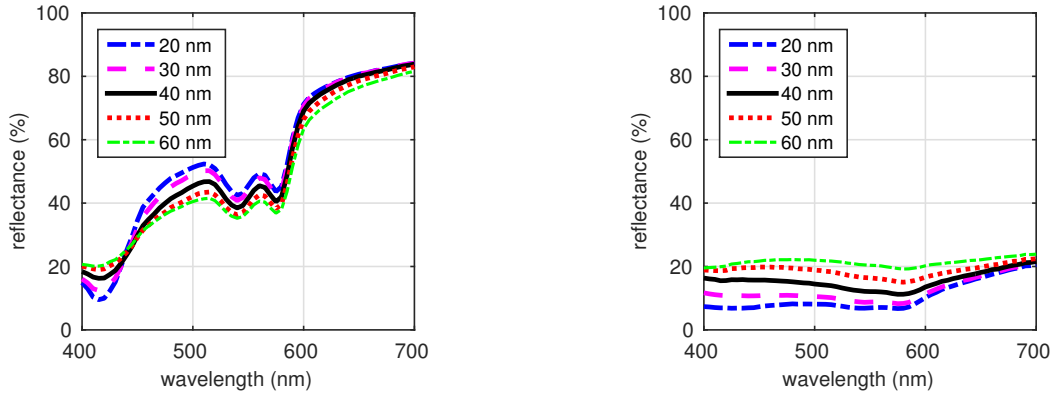

Figure 5.4: Modelled reflectance curves for skin specimens considering varying radius of the fibrils in the papillary dermis (r). (a) Without a subcutaneous vein. (b) With a subcutaneous vein. Note that the baseline skin specimen has $r = 40$ nm.

Now, let us examine Figure 5.5 to see how these observations translate to appearance. In particular, when examining the appearance of the skin specimens with a subcutaneous vein, we can see that decreasing the fibril radius below the baseline value darkens the appearance of the vein and provides a brownish-red or purple coloration. Alternatively, increasing the fibril radius above the baseline value results in a more greenish appearance.

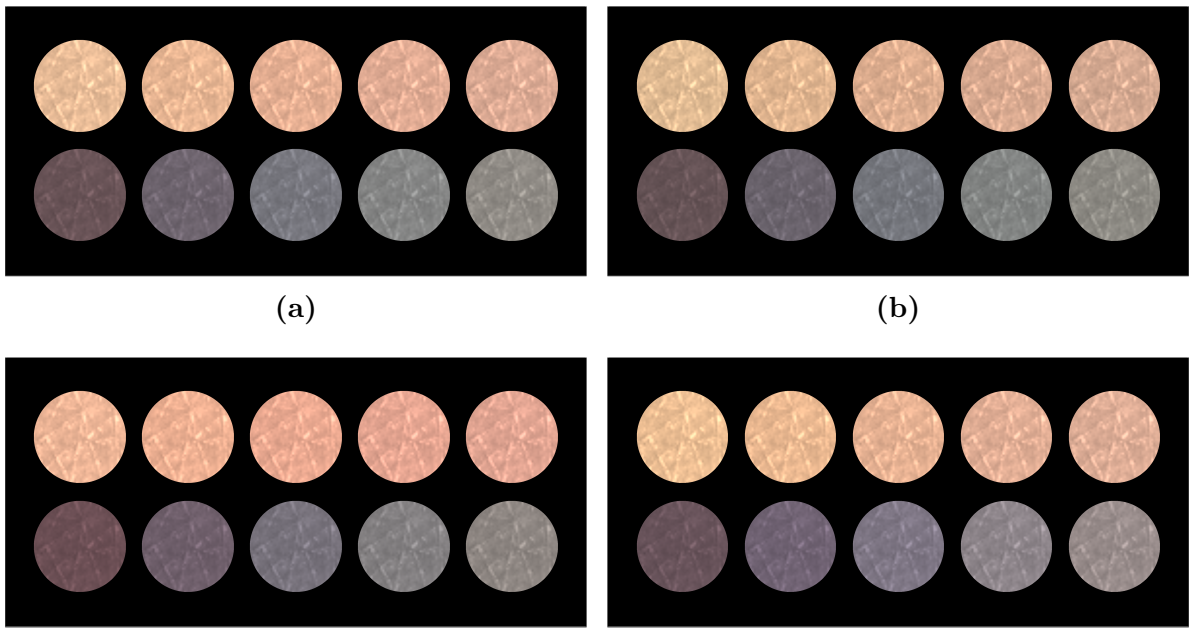

(a) **(b)**

(c) **(d)**

Figure 5.5: Generated swatches depicting variations in skin appearance when modifying the radius of the fibrils in the papillary dermis (r). For comparison purposes, we present swatches for specimens without (top) and with (bottom) a subcutaneous vein in each subfigure. For each subfigure, from left to right: $r = 20$, 30, 40, 50, 60 nm. The swatches were generated considering CIE standard illuminants (a) D50, (b) D65, (c) A and (d) F2. Note that the baseline skin specimen has $r = 40$ nm. The computed RGB triplet values used to generate the swatches in this figure are presented in Table B.4 (Appendix B).

We also performed experiments in which we varied the thickness of the papillary dermis. In the corresponding reflectance curves, presented in Figure 5.6, we can observe similar trends to the experiments in which we varied the fibril radius (Figure 5.4). However, the changes in reflectance are lower in magnitude when varying the papillary dermis thickness given the parameter values that we have selected. Consequently, the corresponding appearance swatches in Figure 5.7 show variations in coloration similar, albeit less prominent, to the results presented in Figure 5.5.

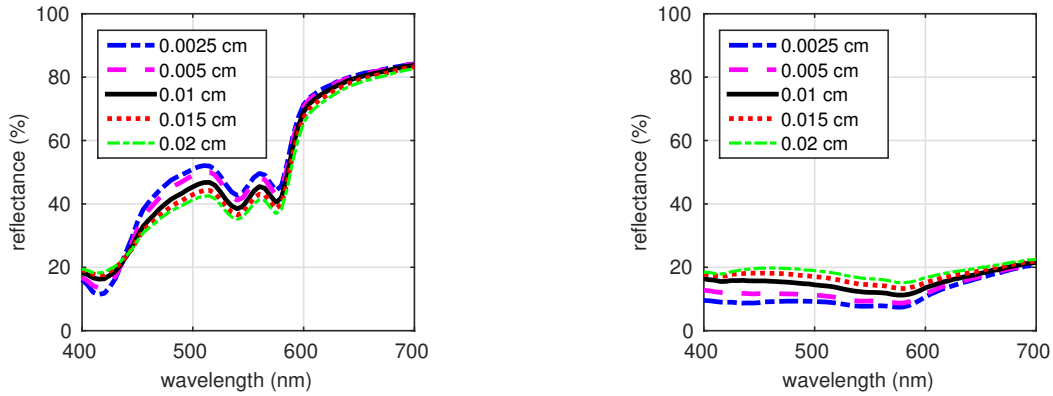

Figure 5.6: Modelled reflectance curves for skin specimens considering varying papillary dermis thickness (t_{PD}). (a) Without a subcutaneous vein. (b) With a subcutaneous vein. Note that the baseline skin specimen has $t_{PD} = 0.02\ cm$.

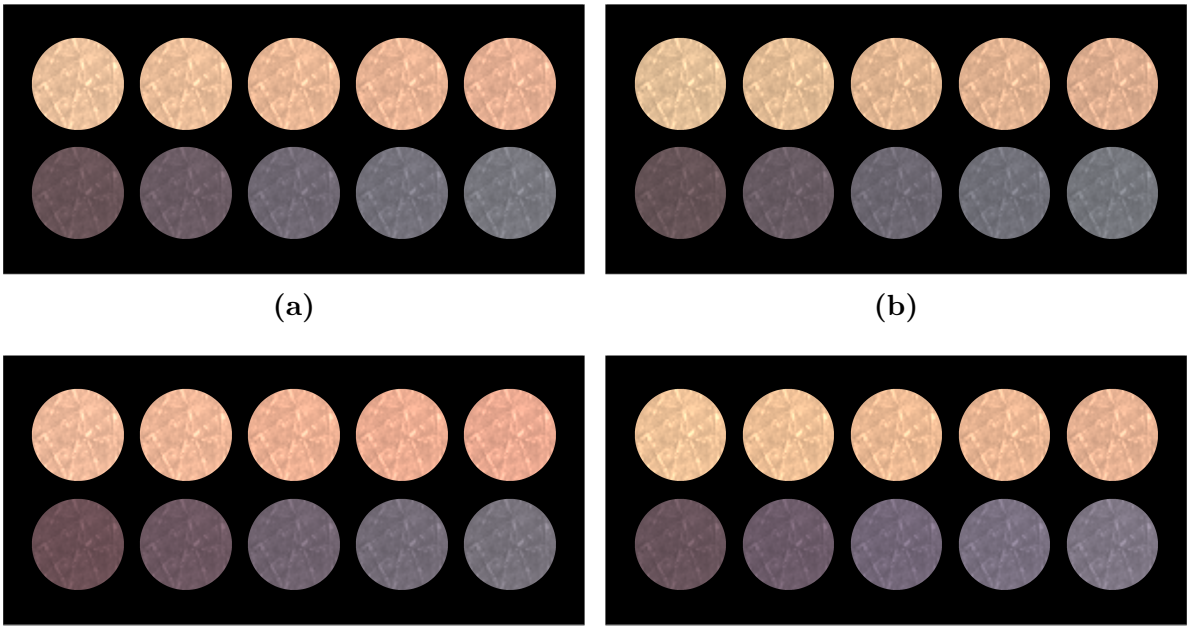

Figure 5.7: Generated swatches depicting variations in skin appearance when modifying the thickness of the papillary dermis (t_{PD}). For comparison purposes, we present swatches for specimens without (top) and with (bottom) a subcutaneous vein in each subfigure. For each subfigure, from left to right: t_{PD} = 0.0025, 0.005, 0.01, 0.015, 0.02 cm. The swatches were generated considering CIE standard illuminants (a) D50, (b) D65, (c) A and (d) F2. Note that the baseline skin specimen has t_{PD} = 0.02 cm. The computed RGB triplet values used to generate the swatches in this figure are presented in Table B.5 (Appendix B).

Now, let us examine the combined effect of varying both the radius of the fibrils and the papillary dermis thickness in Figure 5.8. When examining the swatches that consider Rayleigh scattering (Figure 5.8(a)), we can see that increasing one parameter value while decreasing the other can lead to more subtle changes in the appearance of the specimen, while increasing or decreasing both parameter values simultaneously can lead to more drastic changes in its appearance. On the other hand, when examining the swatches generated with Rayleigh scattering disabled (Figure 5.8(b)), we can verify that similar changes do not take place. This demonstrates that any change in the appearance of a skin specimen with a subcutaneous vein resulting from varying the values of fibril radius and papillary dermis thickness is primarily determined by the occurrence of Rayleigh scattering in this tissue.

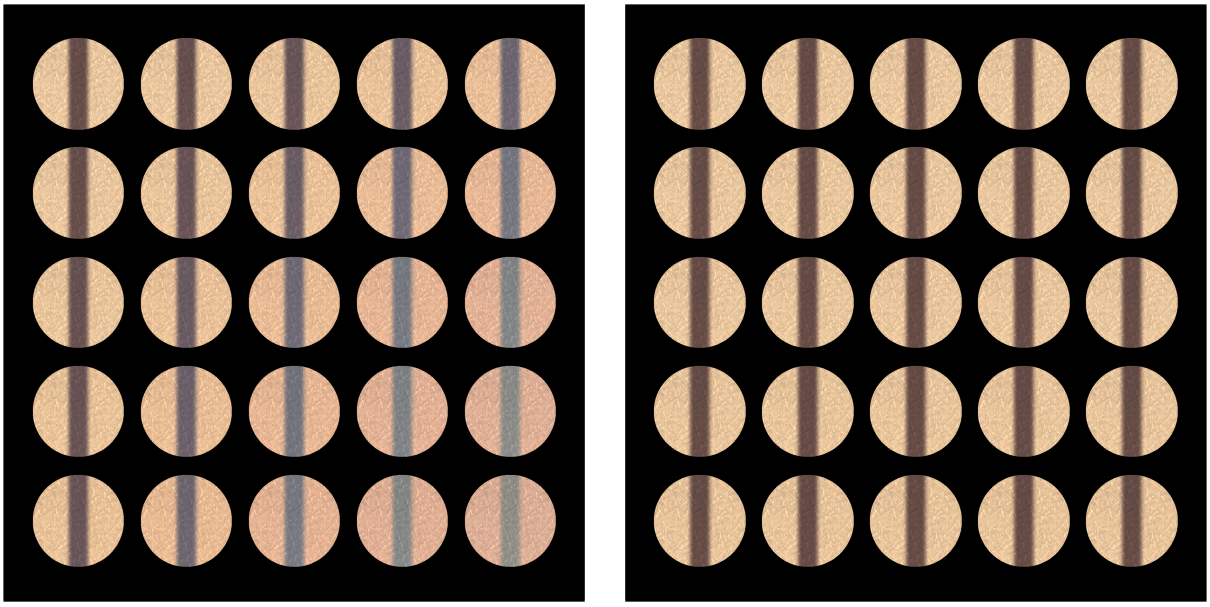

(a) **(b)**

Figure 5.8: Generated swatches depicting several skin specimens with a subcutaneous vein running beneath them considering the CIE standard illuminant D65. Distinct skin specimens were obtained by varying the radius of the fibrils in the papillary dermis (r) and the papillary dermis thickness (t_{PD}). Left to right: $r = 20$, 30, 40, 50, 60 nm. Top to bottom: $t_{PD} = 0.0025$, 0.005, 0.01, 0.015, 0.02 cm. (a) With Rayleigh scattering. (b) Without Rayleigh scattering. Note that the baseline skin specimen has $r = 40$ nm and $t_{PD} = 0.02$ cm. The computed RGB triplet values used to generate the swatches in this figure are presented in Figures B.6 and B.7 (Appendix B).

Chapter 6

Analysis of Research Findings

In this chapter, we present the primary conclusions that can be drawn from our results. We also discuss some of our simulation choices in more detail.

Experiment Set #1 demonstrates that Rayleigh scattering can play a pivotal role in the bluish appearance of veins. Experiment Set #2 shows that varying blood and melanin content within the range of physically plausible concentrations for a lightly pigmented specimen [64] does not affect the significance of the role of Rayleigh scattering in the appearance of veins. Experiment Set #3 demonstrates that the appearance of veins can depend on the morphological characteristics of the papillary dermis. Specifically, any parameter that contributes to the amount of Rayleigh scattering occurring in the papillary dermis (Section 4.3) could potentially affect the appearance of veins.

Although our results obtained in Experiment Set #1 cannot be directly compared to the *in vivo* measurements of Kienle *et al.* [54] because of potential differences in experimental setup and specimen characterization, qualitative comparisons can be made. In particular, their measurements of the amount of light remitted by skin above a visible vein and the adjacent skin tissue shows that one should expect a lower reflectance when performing a measurement above a vein. Furthermore, when considering measurements performed at distinct wavelengths, their data shows that one should expect larger difference in reflectance for longer wavelengths (e.g., 633 nm and 700 nm) than shorter wavelengths (e.g., 450 nm or 500 nm) when comparing skin specimens with and without a subcutaneous vein. Both of these observations can also be verified in our results presented in Figure 5.1(a).

It is also worth noting that we were able to quantitatively reproduce the bluish appearance of veins using standard CIE colour space calculations (Table 5.1(a)), which Kienle *et al.* [54] were unable to achieve using their *in vivo* measurements. As suggested by

themselves, this might be due to the fact that they employed only five reflectance values obtained at close spectral locations. We, on the other hand, considered reflectance values sampled at 61 wavelengths at 5 nm intervals.

Experiment Sec #3 also demonstrates an interesting feature of the fibrils in the papillary dermis. In particular, measurements by Arao *et al.* [8] show that reticulin fibrils in the papillary dermis have a radius in the range 20–25 nm, whereas the collagen fibrils in the papillary dermis have a radius in the range 40–60 nm. Our experiments considering fibrils with 20 nm radius (Figures 5.5 and 5.8(a)) result in veins with a brownish-red to purple appearance. In fact, this observation is similar to the corresponding observation derived from the experiments in which we did not consider Rayleigh scattering (Figure 5.8(b)). Since we fixed the volume fraction of the papillary dermis occupied by fibrils (v_f) and physiologically, reticulin fibrils only make up a fine layer of the papillary dermis [8], Rayleigh scattering caused by reticulin fibrils located in the papillary dermis is unlikely to significantly contribute to the bluish appearance of veins. Therefore, our findings indicate that the Rayleigh scattering (occurring in the papillary dermis) that contributes to the bluish appearance of veins is primarily elicited by collagen fibrils.

In the following sections, we provide some additional considerations regarding our simulation choices and results.

6.1 Intermediate Tissues

In our experiments, we do not fully consider the attenuating properties of the vein wall. We also do not consider a hypodermis between the skin and the vein. In the human body, if a vein is deep enough then scattering in the hypodermis ensures that the vein is not visible. Accordingly, it is possible that a less visually prominent vein may have a thin hypodermal layer between itself and the skin. Although these intermediate tissues may impact the reflectance of skin in general, it is unlikely that they can be the primary source of the a vein's bluish appearance given the optical properties of their main constituents. In the remainder of this section, we examine this claim in more detail.

The weak absorption of visible light in these tissues is dominated by hemoglobin [19, 108, 121]. Since hemoglobin is abundant in the subcutaneous vein, these tissues should have a minor impact on the overall absorptance. However, if we were to consider the effect of hemoglobin in these tissues, it should be similar to increasing the hemoglobin concentration in the reticular dermis. As we can see in Figure 5.3, this does not have a significant effect on the bluish appearance of the vein.

There is also a possibility that small heterogeneous structures in these intermediate tissues produce Rayleigh scattering. However, our experiments indicate that Rayleigh scattering in the skin is strong enough to elicit the bluish appearance of veins without the consideration of these tissues. This is corroborated by the observation that cyanotic fingertips would not appear bluish if Rayleigh scattering in the papillary dermis was not sufficient to prevent blue light from reaching the reticular dermis [15]. Since Rayleigh scattering in the skin occurs before light reaches the hypodermis or vein wall, any additional Rayleigh scattering in these subcutaneous tissues could only increase the, already sufficient, remittance of blue light.

6.2 Vein Appearance

In this work, we have been focusing on the bluish appearance of veins. As demonstrated by Experiment Set #3 (Figures 5.4–5.8), a subcutaneous vein may also appear to be subjectively more green, purple, or grey than blue when considering different physiological states and illumination conditions. These findings indicate that Rayleigh scattering occurring in the papillary dermis can play an important role in the appearance of any visible subcutaneous vein, even though its contribution may not always result in a bluish appearance.

6.3 Pigmentation Level

We have chosen to focus on lightly pigmented specimens in our investigation since melanin absorbs light in the blue region significantly more than in other regions (Figure 2.1(a)). This indicates that additional melanin in the epidermis would increase the absorption of blue light before it reaches the papillary dermis, which would inhibit our ability to examine the effects of Rayleigh scattering caused by the collagen fibrils. We remark, however, that examining the appearance of veins for moderately and highly pigmented specimens may be a topic of interest for future investigation (Chapter 7).

6.4 Venous Blood Characterization

We performed several additional experiments to assess the effect of varying the venous blood characterization on the appearance of a skin specimen with a subcutaneous vein. Since these experiments are tangential to the goal of our investigation, we present these results in Appendix A. When experimenting with various oxygen saturation levels, we observed that variations within a typical physiological range did not have a noticeable impact on coloration. However, arterial oxygenation levels (e.g., 97%) resulted in a skin specimen with a subcutaneous vein reflecting more red light, which, in turn, elicited a purple appearance. Alternatively, extremely low levels of oxygenation levels (e.g., 0%) resulted in less reflected red light, which, in turn, elicited a more dominant blue coloration. We remark that this behaviour is consistent with observations by Kienle *et al.* [54]. We also explored different distributions of red blood cell orientations in the flowing venous blood, corresponding to different shear rates. This did not noticeably affect the resulting coloration.

6.5 Hypodermis Reflectance

In Section 3.2, we mentioned that in our simulations visible light reaching the hypodermis is diffusely reflected back to the reticular dermis. We also noted that this simulation choice was based on reported morphological and optical characteristics of white adipose tissues (Section 2.3) and it is consistent with simulation strategies employed by related works [30,36]. We remark that most of our observations presented in this work (Sections 5 and 6) correspond to a skin specimen with a subcutaneous vein beneath it. Moreover, the direct observation made for a skin specimen with a hypodermis beneath it (Section 5.1) focuses on a feature of skin reflectance curve (Figure 5.1) in the blue region and emphasizes the light that does not reach the hypodermis. Hence, the outcomes of our investigation are not impaired by the simulation choice outlined above.

6.6 Vein Transmittance

In Section 3.3, we mentioned that our simulations discard light rays that are transmitted by the vein. This strategy was motivated by the low probability of light being transmitted by the vein (p^t_{vein}), depicted in the curve presented in Figure 6.1(a). This curve was calculated using the same approach employed for precomputing p^r_{vein} (Figure 4.1), described in Section 3.4. Now, let us consider the worst-case scenario where 100% of light transmitted by the vein would be diffusely remitted by the tissue below. In this case, the amount of light transmitted by the vein and then subsequently remitted by it would be given by $(p^t_{vein})^2$, which is presented in Figure 6.1(b). We note that the maximum value on this curve is 0.53% at 700 nm. This would represent a negligible contribution to the overall reflectance of a skin specimen with a subcutaneous vein (Figure 5.1), notably when compared with the probability of light being reflected by the vein without considering a remission of light by tissues below the vein (Figure 4.1). Hence, the decision of discarding the light rays that might be transmitted by the vein did not affect the observations derived from our *in silico* experiments, especially considering that $(p^t_{vein})^2$ values are even smaller for other wavelengths (Figure 6.1(b)).

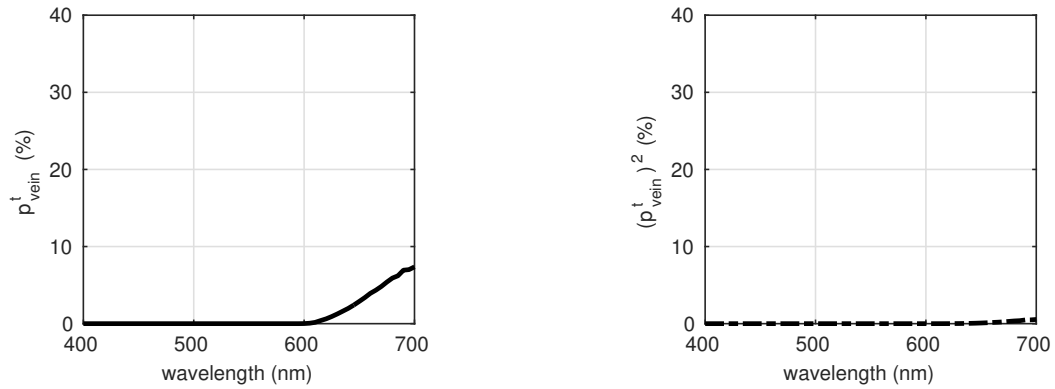

Figure 6.1: Computed transmittance data for the subcutaneous vein specimen employed in our experiments. (a) Probability of light being transmitted by the vein (p^t_{vein}). (b) Squared probability of light being transmitted by the vein ($(p^t_{vein})^2$). The values for p^t_{vein} were computed using an analogous procedure to the precomputation outlined in Section 3.4 considering the blood characterization data presented in Table 4.3.

Chapter 7

Conclusion and Future Work

The *in silico* experimental results presented in this work support the hypothesis that Rayleigh scattering caused by collagen fibrils found in the papillary dermis can play a pivotal role in the bluish appearance of veins. In particular, Rayleigh scattering occurring in the papillary dermis remits blue light from the skin before it can reach the blood flowing through the subcutaneous vein. The blood flowing through the vein then moderately absorbs the red light that reaches it. The net effect of these two optical processes is the bluish appearance of veins. In addition, these results show that distinct vein colorations, such as grey or greenish, may be caused by different amounts of Rayleigh scattering associated with variations in the morphological characteristics of the papillary dermis, notably its thickness and the radius of its collagen fibrils. Finally, our experimental results also indicate that Rayleigh scattering caused by reticulin fibrils located in the papillary dermis is not a significant contributor to the bluish appearance of veins.

As with any *in silico* investigation, the outcomes of our research require confirmation from *in situ* experiments. We remark, however, that our *in silico* experiments were performed using first-principles models, whose predictive capabilities have been extensively evaluated in previous works [29, 116, 124], and considering measured biophysical data provided in the scientific literature. Hence, we are confident that our findings can be corroborated by *in situ* experiments as new technologies that allow measurements to be performed within the papillary dermis under *in vivo* conditions become available.

There are many possibilities for future work. For example, it may be useful to evaluate the impact of the masking effect of melanosomes on the appearance of subcutaneous veins in moderately and darkly pigmented skin specimens, in a similar manner to the work of Baranoski *et al.* regarding cyanosis [16]. In addition to strengthening the current

understanding of fundamental optical mechanisms occurring within the skin, investigations within the realm of the work presented in this thesis could aid in the design of more effective optical devices for the noninvasive detection of physiological changes within the skin and subcutaneous veins. These changes could include, for instance, variations in the concentration of blood-borne substances, such as bilirubin and methemoglobin, associated with the onset of potentially life-threatening conditions like hyperbilirubinemia [99] and methemoglobinemia [11], respectively.

From a visual perspective, a more in-depth exploration of distinct skin specimen characterizations could enable the predictive reproduction of the various skin tones caused by subcutaneous blood vessels. Additionally, placing the vein representation within the cutaneous tissues would allow us to simulate the appearance of enlarged cutaneous vessels. These advancements could contribute to the improvement of computer-generated representations of skin which, in turn, would enhance the effectiveness of scientific, educational and entertainment applications requiring realistic visualizations of the human body.

References

[1] Agache, P. Metrology of the stratum corneum. In *Measuring the Skin*, P. Agache and P. Humbert, Eds. Springer-Berlag, Berlin, Germany, 2004, pp. 101–111.

[2] Agache, P., and Diridollou, S. Subcutis histopathology. In *Measuring the Skin* (Berlin, 2004), P. Agache and P. Humbert, Eds., Springer-Verlag, pp. 401–409.

[3] Agache, P., and Humbert, P. *Measuring the Skin*. Springer, 2004.

[4] Alaluf, S., Atkins, D., Barret, K., Blount, M., Carter, N., and Heath, A. Ethnic variation in melanin content and composition in photoexposed and photoprotected human skin. *Pigment Cell Research 15* (2002), 112–118.

[5] Altshuler, G. B., Anderson, R. R., and Manstein, D. Method and apparatus for the selective targeting of lipid-rich tissues. Patent, 8 2003.

[6] Anderson, R. R., and Parrish, J. A. The optics of human skin. *Journal of Investigative Dermatology 77*, 1 (1981), 13–9.

[7] Anderson, R. R., and Parrish, J. A. Optical properties of human skin. In *The Science of Photomedicine* (N.Y., USA, 1982), J. D. Regan and J. A. Parrish, Eds., Plenun Press, pp. 147–194.

[8] Arao, H., Obata, M., Shimada, T., and Hagisawa, S. Morphological characteristics of the dermal papillae in the development of pressure sores. *Journal of Tissues Viability 8*, 3 (1998), 17–23.

[9] Arifler, D., Pavlova, I., Gillenwater, A., and Richrads-Kortum, R. Light scattering from collagen fiber networks: micro-optical properties of normal and neoplastic stroma. *Biophysical Journal 92* (2007), 3260–3274.

[10] Bain, B. J., Bates, I., Laffan, M. A., and Lewis, S. M. *Dacie and Lewis Practical Haematology*, 11 ed. Elsevier Churchill Livingstone, 2012.

[11] Baranoski, G. V. G., Chen, T. F., Kimmel, B. W., Miranda, E., and Yim, D. On the noninvasive optical monitoring and differentiation of methemoglobinemia and sulfhemoglobinemia. *Journal of Biomedical Optics 17*, 9 (2012), 0970051–09700514.

[12] Baranoski, G. V. G., and Krishnaswamy, A. *Light & Skin Interactions: Simulations for Computer Graphics Applications*. Morgan Kaufmann/Elsevier, Burlington, MA, USA, 2010.

[13] Baranoski, G. V. G., and Rokne, J. *Light Interaction with Plants*. Horwood Publishing, Chichester, 2004.

[14] Baranoski, G. V. G., Rokne, J. G., and Xu, G. Virtual spectrophotometric measurements for biologically and physically based rendering. *The Visual Computer 17*, 8 (2001), 506–518.

[15] Baranoski, G. V. G., Van Leeuwen, S. R., and Chen, T. F. Elucidating the biophysical processes responsible for the chromatic attributes of peripheral cyanosis. In *39th Annual International Conference of the IEEE Engineering in Medicine and Biology Society (EMBC)* (Jeju Island, Korea, August 2017), pp. 90–95.

[16] Baranoski, G. V. G., Van Leeuwen, S. R., and Chen, T. F. On the detection of peripheral cyanosis in individuals with distinct levels of cutaneous pigmentation. In *39th Annual International Conference of the IEEE Engineering in Medicine and Biology Society (EMBC)* (Jeju Island, Korea, August 2017), pp. 4260–4264.

[17] Bashkatov, A. N., Genina, E. A., Kochubey, V. I., l M. Stolnitz, M., Bashkatova, T. A., Novikova, O. V., Peshkova, A. Y., and Tuchin, V. V. Optical properties of melanin in the skin and skinlike phantoms. In *Controlling Tissue Optical Properties: Applications in Clinical Study* (2000), V. V. Tuchin, Ed., vol. 4162, SPIE, pp. 219–226.

[18] Bashkatov, A. N., Genina, E. A., Kochubey, V. I., and Tuchin, V. V. Optical properties of human skin, subcutaneous and mucous tissues in the wavelength range from 400 to 2000 nm. *Journal of Physics D: Applied Physics 38* (2005), 2543–2555.

[19] Bashkatov, A. N., Genina, E. A., and Tuchin, V. V. Optical properties of skin, subcutaneous, and muscle tissues: a review. *Journal of Innovative Optical Health Sciences 4*, 01 (2011), 9–38.

[20] Bianco, S., and Schettini, R. Two new von Kries based chromatic adaptation transforms found by numerical optimization. *Color Research & Application 35*, 3 (2010), 184–192.

[21] Blum, P. Reflectance spectrophotometry and colorimetry. In *Physical Properties Handbook, Ocean Drilling Program* (1997).

[22] Bohren, C. Scattering by particles. In *Handbook of Optics (Volume I: Fundamentals, Techniques, & Design)* (New York, 1995), M. Bass, E. Stryland, D. Williams, and W. Wolfe, Eds., Optical Society of America, McGraw-Hill, Inc., pp. 6.1–6.21. Chapter 6.

[23] Borren, C., and Huffman, D. *Absoprtion and Scattering by Small Particles.* Wiley, N.Y., USA, 1983.

[24] Braverman, I. M. The cutaneous microcirculation. *JID Symposium Proceedings 5*, 1 (2000), 3–9.

[25] Bruls, W. A. G., and Van Der Leun, J. C. Forward scattering properties of human epidermal layers. *Photochemistry and Photobiology 40*, 2 (1984), 231–242.

[26] Butler, W. L. Absorption spectroscopy in vivo theory and application. *Annual Review of Plant Physiology 15*, 1 (1964), 451–460.

[27] Caduff, A., Talary, M. S., and Zakharov, P. Cutaneous blood perfusion as a perturbing factor for noninvasive glucose monitoring. *Diabetes Technology & Therapeutics 12*, 1 (2010), 1–9.

[28] Cerussi, A. E., Berger, A. J., Bevilacqua, F., Shah, N., Jakubowski, D., Butler, J., Holcombe, R. F., and Tromberg, B. J. Sources of absorption and scattering contrast for near-infrared optical mammography. *Academic Radiology 8*, 3 (March 2001), 211–218.

[29] Chen, T. F., Baranoski, G. V. G., Kimmel, B. W., and Miranda, E. Hyperspectral modeling of skin appearance. *ACM Transactions on Graphics 34*, 3 (2015), 31:1–14.

[30] Cotton, S., and Claridge, E. Developing a predictive model of skin colouring. In *SPIE Vol. 2708, Medical Imaging* (1996), pp. 814–825.

[31] Cunnington, A. J., Kendrick, S. F., Wamola, B., Lowe, B., and Newton, C. R. J. C. Carboxyhemoglobin levels in Kenyan children with plasmodium falciparum malaria. *The American Journal of Tropical Medicine and Hygiene 71*, 1 (2004), 43–47.

[32] Cunnington, A. J., Kendrick, S. F. W., Wamola, B., Lowe, B., and Newton, C. R. J. C. Carboxyhemoglobin levels in Kenyan children with plasmodium falciparum malaria. *The American Journal of Tropical Medicine and Hygiene 71*, 1 (2004), 43–47.

[33] de Graaff, K. M. V. *Human Anatomy*, 4th ed. W. C. Brown Publishers, Dubuque, IO, USA, 1995.

[34] Diffey, B. L. A mathematical model for ultraviolet optics in skin. *Physics in Medicine and Biology 28*, 6 (1983), 647–657.

[35] Dinish, U., Wong, C., Sriram, S., Ong, W., Balasundaram, G., Sugii, S., and Olivo, M. Diffuse optical spectroscopy and imaging to detect and quantify adipose tissue browning. *Scientific Reports 7* (2017), 1–12.

[36] Doi, M., and Tominaga, S. Spectral estimation of human skin color using the Kubelka-Munk theory. In *SPIE/IS&T Electronic Imaging* (2003), SPIE, vol. 5008, pp. 221–228.

[37] Donner, C., and Jensen, H. W. A spectral BSSRDF for shading human skin. In *17th Eurographics Workshop on Rendering* (2006), pp. 409–418.

[38] Donner, C., Weyrich, T., d'Eon, E., Ramamoorthi, R., and Rusinkiewicz, S. A layered, heterogeneous reflectance model for acquiring and rendering human skin. *ACM Transactions on Graphics 27*, 5 (2008), 140:1–12.

[39] Edwards, E. A., and Duntley, S. Q. The pigments and color of living human skin. *American Journal of Anatomy 65*, 1 (1939), 1–33.

[40] Findlay, G. Blue skin. *British Journal of Dermatology 83*, 1 (1970), 127–134.

[41] Flewelling, R. Noninvasive optical monitoring. In *The Biomedical Engineering Handbook*, J. D. Bronzino, Ed., 2 ed. CRC Press LLC, 2000.

[42] Flindt, R. *Amazing Numbers in Biology*. Springer, 2006.

[43] Fornage, B. D., and Deshayes, J.-L. Ultrasound of normal skin. *Journal of Clinical Ultrasound 14*, 8 (1986), 619–622.

[44] Fuchs, E. Keratins and the skin. *Annual Review of Cell and Developmental Biology 11*, 1 (1995), 123–154.

[45] Gawkrodger, D. J. *Dermatology An Illustrated Colour Text*. Churchill Livingstone, 2002.

[46] Haymond, S., Cariappa, R., Eby, C. S., and Scott, M. G. Laboratory assessment of oxygenation in methemoglobinemia. *Clinical Chemistry 51*, 2 (2005), 434–444.

[47] Hennessy, A., Oh, C., Diffey, B., Wakamatsu, K., Ito, S., and Rees, J. Eumelanin and pheomelanin concentrations in human epidermis before and after UVB irradiation. *Pigment Cell Research 18* (2005), 220–223.

[48] Hunt, R. W. G. *Measuring Colour*, 2nd ed. Ellis Horwood Limited, Chichester, England, 1991.

[49] International Electrotechnical Commission. Multimedia systems and equipment-color measurement and management-part 2-1: Color management-default RGB color space-sRGB. Technical Report, IEC 61966-2-1, 1999.

[50] Jacques, S. L. Origins of tissue optical properties in the UVA, visible, and NIR regions. *OSA TOPS on Advances in Optical Imaging and Photon Migration 2* (1996), 364–369.

[51] Jacques, S. L. Optical absorption of melanin. Tech. rep., Oregon Medical Laser Center, 2001.

[52] Jacques, S. L., Alter, C. A., and Prahl, S. A. Angular dependence of HeNe laser light scattering by human dermis. *Lasers in the Life Sciences 1* (1987), 309–333.

[53] Jacquez, J. A., Huss, J., McKeehan, W., Dimitroff, J. M., and Kuppenhein, H. F. Spectral reflectance of human skin in the region 0.7-2.6 μ. *Journal of Applied Physiology 8* (1955), 297–299.

[54] Kienle, A., Lilge, L., Vitkin, I. A., Patterson, M. S., Wilson, B. C., Hibst, R., and Steiner, R. Why do veins appear blue? A new look at an old question. *Applied Optics 35*, 7 (1996), 1151–1160.

[55] Kinnunen, M., Kauppila, A., Karmenyan, A., and Myllylä, R. Effect of the size and shape of a red blood cell on elastic light scattering properties at the single-cell level. *Biomedical Optics Express 2*, 7 (2011), 1803–1814.

[56] Kiray, A., Ergür, I., Tayefi, H., Bağriyanik, H. A., and Bacakoğlu, A. K. Anatomical evaluation of the superficial veins of the upper extremity as graft donor source in microvascular reconstructions: a cadaveric study. *Acta Orthopaedica et Traumatologica Turcica 47*, 6 (2012), 405–410.

[57] Klarhöfer, M., Csapo, B., Balassy, C., Szeles, J. C., and Moser, E. High-resolution blood flow velocity measurements in the human finger. *Magnetic Resonance in Medicine 45*, 4 (2001), 716–719.

[58] Kollias, N., Sayre, R. M., Zeise, L., and Chedekel, M. R. Photoprotection by melanin. *Journal of Photochemistry and Photobiology B 9*, 2 (1991), 135–60.

[59] Krishnaswamy, A. BioSpec: A biophysically-based spectral model of light interaction with human skin. Master's thesis, School of Computer Science, University of Waterloo, Waterloo, Ontario, Canada, 2005.

[60] Land, E. H., and McCann, J. J. Lightness and retinex theory. *Josa 61*, 1 (1971), 1–11.

[61] Latimer, P. A wave-optics effect which enhances light absorption by chlorophyll *in vivo*. *Photochemistry and Photobiology 40*, 2 (1984), 193–199.

[62] Lee, R., Mathews-Roth, M. M., Pathak, M. A., and Parrish, J. A. The detection of carotenoid pigments in human skin. *Journal of Investigative Dermatology 64*, 3 (03 1975), 175–177.

[63] Lindberg, L.-G., and Oberg, P. A. Optical properties of blood in motion. *Optical Engineering 32*, 2 (1993), 253–257.

[64] Lister, T. *Simulating the Color of Port Wine Stain Skin.* PhD thesis, University of Southampton,U. K., February 2013.

[65] Lister, T., Wright, P. A., and Chappell, P. H. Optical properties of human skin. *Journal of Biomedical Optics 17*, 9 (2012), 090901–1–14.

[66] Lovell, A. T., Hebden, J. C., Goldstone, J. C., and Cope, M. Determination of the transport scattering coefficient of red blood cells. In *Proc. SPIE 3597, Optical Tomography and Spectroscopy of Tissue III* (1999), vol. 3597, pp. 175–182.

[67] Magnenat-Thalmann, N., Kalra, P., L. Leveque, J., Bazin, R., Batisse, D., and Querleux, B. A computational skin model: fold and wrinkle formation. *IEEE Transactions on Information Technology in Biomedicine 6*, 4 (2002), 317–323.

[68] McCartney, E. J. *Optics of the Atmosphere: Scattering by Molecules and Particles*. John Wiley & Sons, 1976.

[69] Meinke, M., Müller, G., Helfmann, J., and Friebel, M. Optical properties of platelets and blood plasma and their influence on the optical behavior of whole blood in the visible to near infrared wavelength range. *Journal of Biomedical Optics 12*, 1 (2007), 014024–014024.

[70] Meyer-Arendt, J. R. *Introduction to Modern and Classical Optics*. Prentice-Hall, New Jersey, 1984.

[71] Mokken, F. C., van der Waart, F. J. M., Henny, C. P., Goedhart, P. T., and Gelb, A. W. Differences in peripheral arterial and venous hemorheologic parameters. *Annals of Hematology 73*, 3 (1996), 135–137.

[72] Nakagawa, N., Matsumoto, M., and Sakai, S. *In vivo* measurement of the water content in the dermis by confocal Raman spectroscopy. *Skin Research and Technology 16*, 2 (2010), 137–141.

[73] Natural Phenomena Simulation Group (NPSG). Human Blood Data. http://www.npsg.uwaterloo.ca/data/blood.php, February 2017.

[74] Natural Phenomena Simulation Group (NPSG). Human Skin Data. http://www.npsg.uwaterloo.ca/data/skin.php, February 2017.

[75] Natural Phenomena Simulation Group (NPSG). NPSGD Framework. http://www.npsg.uwaterloo.ca/models/npsgd_software.php, May 2017.

[76] Natural Phenomena Simulation Group (NPSG). Run CLBlood Online. http://www.npsg.uwaterloo.ca/models/clblood.php, May 2017.

[77] Natural Phenomena Simulation Group (NPSG). Run HyLIoS Online. http://www.npsg.uwaterloo.ca/models/hylios.php, May 2017.

[78] Nielsen, K. P., Zhao, L., Stamnes, J. J., Stamnes, K., and Moan, J. Reflectance spectra of pigmented and nonpigmented skin in the UV spectral region. *Photochemistry and Photobiology 80* (2004), 450–455.

[79] Noll, M. L., and Byers, J. F. Usefulness of measures of Svo_2, Spo_2, vital signs, and derived dual oximetry parameters as indicators of arterial blood gas variables during weaning of cardiac surgery patients from mechanical ventilation. *Heart & Lung 24*, 3 (1995), 220–227.

[80] Oettlé, A. The blue scrotum of the vervet monkey. *The South African Journal of Medical Sciences 23* (1958), 225–230.

[81] Olson, R. L., Gaylor, J., and Everett, M. A. Skin color, melanin, and erythema. *Arch. Dermatol. 108*, 4 (1973), 541–544.

[82] Palmer, K. F., and Williams, D. Optical properties of water in the near infrared. *Journal of the Optical Society of America 64*, 8 (Aug 1974), 1107–1110.

[83] Papaioannou, T. G., and Stefanadis, C. Vascular wall shear stress: basic principles and methods. *Hellenic J Cardiol 46*, 1 (2005), 9–15.

[84] Pathak, M. A. Functions of melanin and protection by melanin. In *Melanin: Its Role in Human Photoprotection* (Overland Park, Kansas, USA, 1995), M. R. C. L. Zeise and T. B. Fitzpatrick, Eds., Valdenmar Publishing Co., pp. 125–134.

[85] Plewig, G., Scheuber, E., Reuter, B., and Waidelich, W. Thickness of the corneocytes. In *Stratum Corneum* (Berlin, 1983), R. Marks and G. Plewig, Eds., Springer-Verlag, pp. 171–174.

[86] Pope, R. M., and Fry, E. S. Absorption spectrum (380–700 nm) of pure water. II. Integrating cavity measurements. *Applied Optics 36*, 33 (Nov 1997), 8710–8723.

[87] Prahl, S. A. *Light Transport in Tissue*. PhD thesis, The University of Texas at Austin, USA, December 1988.

[88] Prahl, S. A. Optical absorption of hemoglobin. Tech. rep., Oregon Medical Laser Center, 1999.

[89] Prahl, S. A. PhotochemCAD spectra by category. Tech. rep., Oregon Medical Laser Center, 2001.

[90] Querleux, B., Darrasse, L., and Bittoun, J. Magnetice resonance imaging of human skin in vivo. In *Bioengineering of the Skin Skin Imaging and Analysis* (Boca Raton, FL, USA, 2007), K. Wilhelm, E. Berardesca, P. Elsner, and H. I. Maibach, Eds., CRC Press, pp. 99–109.

[91] Randeberg, L. L., Bonesrønning, J. H., Dalaker, M., Nelson, J. S., and Svaasand, L. O. Methemoglobin formation during laser induced photothermolysis of vascular skin lesions. *Lasers in Surgery and Medicine 34*, 5 (2004), 414–419.

[92] Robertson, K., and Rees, J. L. Variation in epidermal morphology in human skin at different body sites as measured by reflectance confocal microscopy. *Acta Derm. Venereol. 90* (2010), 368–373.

[93] Robertson, K., and Rees, J. L. Variation in epidermal morphology in human skin at different body sites as measured by reflectance confocal microscopy. *Acta dermatovenereologica 90*, 4 (2010), 368–373.

[94] Robertson, P., and Schonhut, J. Color in computer graphics. *IEEE Computer Graphics and Applications 19*, 4 (1999), 18–19.

[95] Roggan, A., Dorschel, K., Minet, O., Wolff, D., and Müller, G. The optical properties of biological tissue in the near infrared wavelength range. *Laser-induced Interstitial Therapy. SPIE Press, Bellingham, WA* (1995), 10–44.

[96] Rolinski, B., Küster, H., Ugele, B., Gruber, R., and Horn, K. Total bilirubin measurement by photometry on a blood gas analyzer: Potential for use in neonatal testing at the point of care. *Clinical Chemistry 47*, 10 (2001), 1845–1847.

[97] S. Haymond, R. Cariappa, C. S. E., and Scott, M. G. Laboratory assessment of oxygenation in methemoglobinemia. *Clinical Chemistry 51*, 2 (2005), 434–444.

[98] Saidi, I., Jacques, S., and Tittel, F. Mie and Rayleigh modeling of visible-light scattering in neonatal skin. *Applied Optics 34*, 31 (November 1995), 7410–7418.

[99] Saidi, I. S. *Transcutaneous optical measurement of hyperbilirubinemia in neonates.* PhD thesis, Rice University, 1992.

[100] Schmitt, J., Knüttel, A., and Bonner, R. Measurement of optical properties of biological tissues by low-cogerence reflectometry. *Applied Optics 32*, 30 (1993), 6032–6041.

[101] Shimizu, H. *Shimizu's Textbook of Dermatology*. Hokkaido University Press, 2007.

[102] Siggaard-Andersen, O., Nørgaard-Pedersen, B., and Rem, J. Hemoglobin pigments. spectrophotometric determination of oxy-, carboxy-, met-, and sulfhemoglobin in capillary blood. *Clinica Chimica Acta 42*, 1 (1972), 85 – 100.

[103] Squier, C. A., Cox, P., and Wertz, P. W. Lipid content and water permeability of skin and oral mucosa. *Journal of Investigative Dermatology 96*, 1 (1991), 123–126.

[104] Strutt, J. W. On the scattering of light by small particles. *Philosophical Magazine 41*, 275 (June 1871), 447–454.

[105] Strutt, J. W. On the transmission of light through an atmosphere containing many small particles in suspension, and on the origin of the blue of the sky. *Philosophical Magazine 47*, 287 (April 1899), 375–384.

[106] Sun, J., Bhushan, B., and Tong, J. Structural coloration in nature. *Rsc Advances 3*, 35 (2013), 14862–14889.

[107] Susstrunk, S. E., Holm, J. M., and Finlayson, G. D. Chromatic adaptation performance of different RGB sensors. In *Color Imaging: Device-Independent Color, Color Hardcopy, and Graphic Arts VI* (2000), vol. 4300, International Society for Optics and Photonics, pp. 172–184.

[108] Švejcar, J., Přerovskỳ, I., Linhart, J., and Kruml, J. Content of collagen, elastin, and water in walls of the internal saphenous vein in man. *Circulation Research 11*, 2 (1962), 296–300.

[109] Szabo, G., Gerald, A., Pathak, M., and Fitzpatrick, T. B. Racial differences in the fate of melanosomes in human epidermis. *Nature 222*, 5198 (06 1969), 1081–1082.

[110] Talreja, P. S., Kasting, G. B., Kleene, N. K., Pickens, W. L., and Wang, T. Visualization of the lipid barrier and measurement of lipid pathlength in human stratum corneum. *AAPS PharmSci 3*, 2 (2001), 48–56.

[111] Tearney, G. J., Brezinski, M. E., Southern, J. F., Bouma, B. E., Hee, M. R., and Fujimoto, J. G. Determination of the refractive index of highly scattering human tissue by optical coherence tomography. *Optics Letters 20*, 21 (Nov 1995), 2258–2260.

[112] Thody, A. J., Higgins, E. M., Wakamatsu, K., Ito, S., Burchill, S. A., and Marks, J. M. Pheomelanin as well as eumelanin is present in human epidermis. *Journal of Investigative Dermatology 97*, 2 (08 1991), 340–344.

[113] Tuchin, V. V. *Tissue Optics: Light Scattering Methods and Instruments for Medical Diagnosis*. SPIE PM. SPIE/International Society for Optical Engineering, 2007.

[114] van Gemert, M., Jacques, S., Sterenborg, H., and Star, W. Skin optics. *IEEE Transactions on Biomedical Engineering 36*, 12 (1989), 1146–1154.

[115] Van Leeuwen, S. R., and Baranoski, G. V. G. Identifying the optical phenomena responsible for the blue appearance of veins. In *2017 Optical Engineering + Applications Conference: Light in Nature VI* (San Diego, August 2017), vol. 10367, International Society for Optics and Photonics, pp. 103670F–1–15.

[116] Van Leeuwen, S. R., Baranoski, G. V. G., and Kimmel, B. W. Revisiting the CLBlood model: Formulation enhancements and online deployment. Technical Report CS-2017-01, School of Computer Science, University of Waterloo, February 2017.

[117] Varcoe, J. S. *Clinical Biochemistry: Techniques and Instrumentation : A Practical Course*. World Scientific, 2001.

[118] Viator, J. A., Komadina, J., Svaasand, L. O., Aguilar, G., Choi, B., and Stuart, N. J. A comparative study of photoacoustic and reflectance methods for determination of epidermal melanin content. *Journal of Investigative Dermatology 122*, 6 (06 2004), 1432–1439.

[119] Wang, X., Milner, T. E., and anf J. S. Nelson, M. C. C. Group refractive index measurement of dry and hydrated type I collagen films using optical low-coherence reflectometry. *Journal of Biomedical Optics 12* (1996), 212–216.

[120] Williams, M. L., Hincenbergs, M., and Holbrook, K. A. Skin lipid content during early fetal development. *Journal of Investigative Dermatology 91*, 3 (09 1988), 263–268.

[121] Yang, M. F., Tuchin, V. V., and Yaroslavsky, A. N. Principles of light-skin interactions. In *Light-Based Therapies for Skin of Color* (London, 2009), E. D. Baron, Ed., Springer-Verlag, pp. 1–44.

[122] Yarynovska, I. H., and Bilyi, A. I. Absorption spectra of sulfhemoglobin derivates of human blood. In *Biomedical Optics 2006* (2006), International Society for Optics and Photonics.

[123] Yarynovska, I. H., and Bilyi, A. I. Absorption spectra of sulfhemoglobin derivatives of human blood. In *Optical Diagnostics and Sensing VI* (2006), G. L. Cote and A. V. Priezzhev, Eds., vol. 6094, SPIE, pp. 1–6.

[124] Yim, D., Baranoski, G. V. G., Kimmel, B. W., Chen, T. F., and Miranda, E. A cell-based light interaction model for human blood. In *Computer Graphics Forum* (2012), vol. 31, Wiley Online Library, pp. 845–854.

[125] Young, A. R. Chromophores in human skin. *Physics in Medicine and Biology 42*, 5 (1997), 789.

[126] Yoxall, C. W., and Weindling, A. M. Measurement of venous oxyhaemoglobin saturation in the adult human forearm by near infrared spectroscopy with venous occlusion. *Medical and Biological Engineering and Computing 35*, 4 (1997), 331–336.

APPENDICES

Appendix A

Supplemental Experimental Results

The results presented in this appendix correspond to the experiments and observations discussed in Section 6.4. The experiments with varying venous blood oxygenation (SaO_2), presented in Figure A.1, considered ratios of oxyhemoglobin to deoxyhemoglobin ranging from 0% to 100%. Note that in these experiments the other (dysfunctional) hemoglobin concentrations remained constant, i.e., we used the values presented in Table 4.3.

The experiments with varying orientation of the individual red blood cells, presented in Figure A.2, correspond to the various extremes of the possible flow states. The "flowing" sample is the default state considered in Table 4.3. The "aligned", "rolling" and "random" samples indicate that 100% of the red blood cells are aligned with the flow direction, rolling or randomly oriented, respectively. For more information on these flow states, refer to our previous publications describing CLBlood [116, 124].

To accommodate colour-blind readers, Appendix B provides RGB triplet values for all generated colour swatches presented in this chapter.

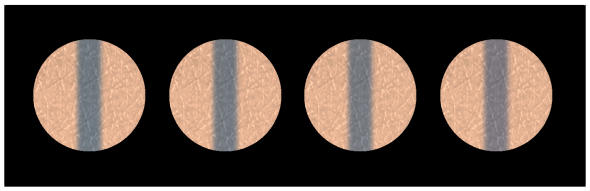

Figure A.1: Generated swatches depicting several skin specimens with a subcutaneous vein running beneath them considering the CIE standard illuminant D65. Distinct skin specimens were obtained by varying the oxygenation (SaO_2) of the blood flowing through the subcutaneous vein. Left to right: $SaO_2 = 0\%$, 50%, 70%, 100%. Note that the baseline oxygenation is $SaO_2 = 70\%$. The computed RGB triplet values used to generate the swatches in this figure are presented in Table B.8 (Appendix B).

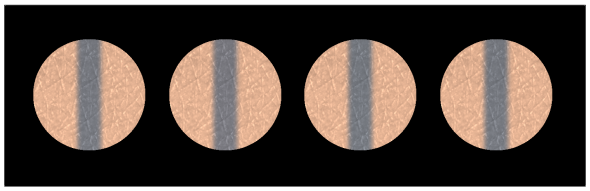

Figure A.2: Generated swatches depicting several skin specimens with a subcutaneous vein running beneath them considering the CIE standard illuminant D65. Distinct skin specimens were obtained by varying the orientation of the individual red blood cells within the subcutaneous vein. Left to right: orientation distribution = "flowing", "aligned", "rolling", "random". Note that the baseline state is "flowing". The computed RGB triplet values used to generate the swatches in this figure are presented in Table B.9 (Appendix B).

Appendix B

Tables of RGB Values

In this appendix, we present the RGB values that were calculated using the procedure outlined in Appendix C during the swatch generation process (Section 4.4) for the figures in Section 5 and Appendix A.

Table B.1: The RGB (Red, Green, Blue) triplets employed in the generation of the swatches presented in Figure 5.2. (a) With Rayleigh scattering. (b) Without Rayleigh scattering. Note that this is a copy of Table 5.1, presented again for the convenience of the reader.

Illuminant	Skin	Skin + Vein
D50	(242, 191, 159)	(124, 125, 133)
D65	(234, 189, 155)	(121, 124, 131)
A	(256, 185, 156)	(124, 119, 129)
F2	(245, 194, 159)	(132, 124, 139)

(a)

Illuminant	Skin	Skin + Vein
D50	(245, 208, 173)	(108, 78, 73)
D65	(237, 206, 168)	(103, 77, 72)
A	(248, 200, 171)	(111, 74, 72)
F2	(251, 210, 170)	(105, 79, 75)

(b)

Table B.2: The RGB (Red, Green, Blue) triplets employed in the generation of the swatches presented in Figure 5.3(a). (a) $f_{mel} = 1.0$. (b) $f_{mel} = 1.5$. (c) $f_{mel} = 2.0$. (d) $f_{mel} = 2.5$.

f_{bl}	Skin	Skin + Vein
1.0	(237, 206, 168)	(103, 77, 72)
1.5	(234, 198, 157)	(103, 77, 71)
2.0	(231, 190, 148)	(103, 76, 71)
2.5	(229, 184, 141)	(103, 76, 70)

(a)

f_{bl}	Skin	Skin + Vein
1.0	(231, 199, 160)	(102, 77, 71)
1.5	(228, 191, 150)	(102, 76, 71)
2.0	(225, 184, 142)	(102, 76, 70)
2.5	(223, 178, 135)	(102, 75, 70)

(b)

f_{bl}	Skin	Skin + Vein
1.0	(225, 192, 153)	(101, 76, 71)
1.5	(222, 185, 144)	(101, 76, 70)
2.0	(219, 179, 137)	(101, 75, 70)
2.5	(217, 173, 131)	(101, 75, 70)

(c)

f_{bl}	Skin	Skin + Vein
1.0	(220, 187, 147)	(100, 76, 70)
1.5	(217, 180, 138)	(101, 75, 70)
2.0	(215, 174, 132)	(100, 75, 70)
2.5	(213, 168, 126)	(100, 74, 70)

(d)

Table B.3: The RGB (Red, Green, Blue) triplets employed in the generation of the swatches presented in Figure 5.3(b). (a) $f_{mel} = 1.0$. (b) $f_{mel} = 1.5$. (c) $f_{mel} = 2.0$. (d) $f_{mel} = 2.5$.

f_{bl}	Skin	Skin + Vein
1.0	(234, 189, 155)	(121, 124, 131)
1.5	(231, 181, 149)	(121, 123, 130)
2.0	(228, 174, 145)	(121, 123, 129)
2.5	(225, 168, 141)	(121, 122, 129)

(a)

f_{bl}	Skin	Skin + Vein
1.0	(227, 182, 147)	(120, 121, 126)
1.5	(224, 174, 142)	(120, 121, 125)
2.0	(221, 168, 138)	(120, 120, 125)
2.5	(219, 163, 135)	(120, 120, 124)

(b)

f_{bl}	Skin	Skin + Vein
1.0	(221, 176, 141)	(119, 119, 122)
1.5	(218, 169, 136)	(119, 118, 121)
2.0	(215, 163, 133)	(119, 118, 120)
2.5	(213, 158, 130)	(119, 118, 120)

(c)

f_{bl}	Skin	Skin + Vein
1.0	(216, 171, 135)	(118, 116, 118)
1.5	(213, 164, 131)	(118, 116, 117)
2.0	(210, 158, 128)	(118, 116, 117)
2.5	(208, 154, 126)	(118, 116, 116)

(d)

Table B.4: The RGB (Red, Green, Blue) triplets employed in the generation of the swatches presented in Figure 5.5. The values were generated considering CIE standard illuminants (a) D50, (b) D65, (c) A and (d) F2.

r (nm)	Skin	Skin + Vein
20	(243, 196, 158)	(109, 87, 91)
30	(242, 190, 153)	(114, 104, 115)
40	(239, 182, 153)	(124, 124, 132)
50	(234, 178, 154)	(138, 139, 138)
60	(230, 178, 155)	(149, 145, 139)

(a)

r (nm)	Skin	Skin + Vein
20	(234, 195, 153)	(105, 86, 89)
30	(234, 188, 149)	(111, 103, 113)
40	(231, 181, 149)	(121, 123, 130)
50	(226, 177, 150)	(135, 137, 136)
60	(222, 176, 151)	(146, 143, 137)

(b)

r (nm)	Skin	Skin + Vein
20	(247, 189, 157)	(112, 83, 88)
30	(247, 183, 152)	(116, 99, 112)
40	(244, 176, 150)	(124, 119, 128)
50	(239, 172, 151)	(136, 133, 134)
60	(234, 171, 152)	(147, 140, 135)

(c)

r (nm)	Skin	Skin + Vein
20	(246, 198, 154)	(109, 87, 95)
30	(245, 192, 151)	(117, 103, 120)
40	(240, 185, 153)	(131, 123, 138)
50	(235, 181, 155)	(147, 138, 144)
60	(231, 180, 156)	(158, 146, 144)

(d)

Table B.5: The RGB (Red, Green, Blue) triplets employed in the generation of the swatches presented in Figure 5.7. The values were generated considering CIE standard illuminants (a) D50, (b) D65, (c) A and (d) F2.

t_{PD} (cm)	Skin	Skin + Vein
0.0025	(244, 200, 162)	(109, 87, 92)
0.005	(244, 197, 159)	(111, 95, 104)
0.01	(241, 186, 153)	(120, 118, 128)
0.015	(243, 190, 155)	(116, 108, 120)
0.02	(239, 182, 153)	(124, 124, 132)

(a)

t_{PD} (cm)	Skin	Skin + Vein
0.0025	(235, 198, 157)	(105, 86, 90)
0.005	(235, 195, 154)	(108, 94, 103)
0.01	(233, 184, 150)	(117, 117, 126)
0.015	(234, 189, 151)	(112, 107, 118)
0.02	(231, 181, 149)	(121, 123, 130)

(b)

t_{PD} (cm)	Skin	Skin + Vein
0.0025	(248, 192, 161)	(112, 83, 89)
0.005	(248, 189, 157)	(114, 91, 102)
0.01	(246, 179, 151)	(120, 112, 124)
0.015	(247, 184, 153)	(117, 103, 116)
0.02	(244, 176, 150)	(124, 119, 128)

(c)

t_{PD} (cm)	Skin	Skin + Vein
0.0025	(248, 202, 158)	(109, 87, 96)
0.005	(247, 199, 156)	(113, 95, 110)
0.01	(243, 188, 153)	(126, 116, 134)
0.015	(245, 193, 153)	(120, 107, 126)
0.02	(240, 185, 153)	(131, 123, 138)

(d)

Table B.6: The RGB (Red, Green, Blue) triplets employed in the generation of the swatches presented in Figure 5.8(a). (a) $r = 20$. (b) $r = 30$. (c) $r = 40$. (d) $r = 50$. (e) $r = 60$.

t_{PD} (cm)	Skin	Skin + Vein
0.0025	(235, 200, 160)	(103, 78, 74)
0.005	(235, 200, 159)	(104, 80, 77)
0.01	(235, 198, 157)	(104, 82, 82)
0.015	(235, 197, 155)	(105, 84, 86)
0.0025	(234, 195, 153)	(105, 86, 89)

(a)

t_{PD} (cm)	Skin	Skin + Vein
0.0025	(235, 200, 159)	(104, 81, 80)
0.005	(235, 198, 157)	(105, 85, 88)
0.01	(235, 195, 154)	(107, 92, 99)
0.015	(235, 191, 151)	(109, 98, 107)
0.0025	(234, 188, 149)	(111, 103, 113)

(b)

t_{PD} (cm)	Skin	Skin + Vein
0.0025	(235, 198, 157)	(105, 86, 90)
0.005	(235, 195, 154)	(108, 94, 103)
0.01	(234, 189, 151)	(112, 107, 118)
0.015	(233, 184, 150)	(117, 117, 126)
0.0025	(231, 181, 149)	(121, 123, 130)

(c)

t_{PD} (cm)	Skin	Skin + Vein
0.0025	(236, 196, 155)	(108, 94, 102)
0.005	(235, 190, 152)	(112, 107, 118)
0.01	(232, 183, 151)	(121, 123, 131)
0.015	(228, 179, 150)	(129, 132, 134)
0.0025	(226, 177, 150)	(135, 137, 136)

(d)

t_{PD} (cm)	Skin	Skin + Vein
0.0025	(235, 192, 153)	(111, 104, 115)
0.005	(233, 185, 152)	(119, 120, 129)
0.01	(228, 179, 152)	(132, 135, 136)
0.015	(224, 177, 151)	(141, 141, 137)
0.0025	(222, 176, 151)	(146, 143, 137)

(e)

Table B.7: The RGB (Red, Green, Blue) triplets employed in the generation of the swatches presented in Figure 5.8(b). (a) $r = 20$. (b) $r = 30$. (c) $r = 40$. (d) $r = 50$. (e) $r = 60$.

t_{PD} (cm)	Skin	Skin + Vein
0.0025	(235, 200, 160)	(103, 77, 71)
0.005	(235, 200, 160)	(103, 77, 71)
0.01	(235, 199, 159)	(103, 77, 71)
0.015	(234, 198, 158)	(103, 77, 71)
0.0025	(234, 198, 157)	(103, 77, 71)

(a)

t_{PD} (cm)	Skin	Skin + Vein
0.0025	(235, 200, 160)	(103, 77, 71)
0.005	(235, 200, 160)	(103, 77, 71)
0.01	(235, 199, 159)	(103, 77, 71)
0.015	(234, 198, 158)	(103, 77, 71)
0.0025	(234, 198, 157)	(103, 77, 71)

(b)

t_{PD} (cm)	Skin	Skin + Vein
0.0025	(235, 200, 160)	(103, 77, 71)
0.005	(235, 200, 160)	(103, 77, 71)
0.01	(235, 199, 159)	(103, 77, 71)
0.015	(234, 198, 158)	(103, 77, 71)
0.0025	(234, 198, 157)	(103, 77, 71)

(c)

t_{PD} (cm)	Skin	Skin + Vein
0.0025	(235, 200, 160)	(103, 77, 71)
0.005	(235, 200, 160)	(103, 77, 71)
0.01	(235, 199, 159)	(103, 77, 71)
0.015	(234, 198, 158)	(103, 77, 71)
0.0025	(234, 198, 157)	(103, 77, 71)

(d)

t_{PD} (cm)	Skin	Skin + Vein
0.0025	(235, 200, 160)	(103, 77, 71)
0.005	(235, 200, 160)	(103, 77, 71)
0.01	(235, 199, 159)	(103, 77, 71)
0.015	(234, 198, 158)	(103, 77, 71)
0.0025	(234, 198, 157)	(103, 77, 71)

(e)

Table B.8: The RGB (Red, Green, Blue) triplets employed in the generation of the swatches presented in Figure A.1.

SaO_2 (%)	Skin	Skin + Vein
0	(231, 181, 149)	(115, 124, 131)
50	(231, 181, 149)	(118, 124, 130)
70	(231, 181, 149)	(121, 124, 130)
100	(231, 181, 149)	(128, 123, 130)

Table B.9: The RGB (Red, Green, Blue) triplets employed in the generation of the swatches presented in Figure A.2.

Orientation	Skin	Skin + Vein
Flowing	(231, 181, 149)	(121, 124, 130)
Aligned	(231, 181, 149)	(124, 124, 130)
Rolling	(231, 181, 149)	(120, 124, 130)
Random	(231, 181, 149)	(121, 124, 130)

Appendix C

Spectral Reflectance to sRGB Conversion Procedure

This appendix outlines the procedure used to convert the reflectance data obtained in our experiments to the sRGB values used in the swatch generation process (Section 4.4).

First, we convert the spectral reflectance data to CIE XYZ values using the following equations [21]:

$$\begin{aligned} X &= K \sum_{\lambda=400}^{700} S(\lambda)x(\lambda)R(\lambda), \\ Y &= K \sum_{\lambda=400}^{700} S(\lambda)y(\lambda)R(\lambda), \\ Z &= K \sum_{\lambda=400}^{700} S(\lambda)z(\lambda)R(\lambda) \end{aligned} \tag{C.1}$$

where $x(\lambda)$, $y(\lambda)$ and $z(\lambda)$ are CIE 1931 colour-matching functions (two-degree observer), $S(\lambda)$ is the spectral power distribution of the illuminant, $R(\lambda)$ is the spectral reflectance, and K is defined as:

$$K = \frac{100}{\sum_{\lambda=400}^{700} S(\lambda)y(\lambda)}. \tag{C.2}$$

After computing the XYZ tristimulus values, the corresponding sRGB triplet can be calculated using the procedure outlined in the remainder of this appendix [49, 94].

First, we calculate intermediate sRGB values R_l, G_l and B_l using the following equation [49, 94]:

$$\begin{bmatrix} R_l \\ G_l \\ B_l \end{bmatrix} = \begin{bmatrix} 3.2404542 & -1.5371385 & -0.4985314 \\ -0.9692660 & 1.8760108 & 0.0415560 \\ 0.0556434 & -0.2040259 & 1.0572252 \end{bmatrix} \begin{bmatrix} X \\ Y \\ Z \end{bmatrix}, \tag{C.3}$$

These intermediate values are then used to compute the sRGB triplet [49, 94], assuming the use of the CIE standard illuminant D65 [48]:

$$\begin{aligned} R &= \begin{cases} 12.92R_l & R_l \leq 0.0031308 \\ 1.055R_l^{\frac{1}{2.4}} - 0.055 & R_l > 0.0031308 \end{cases}, \\ G &= \begin{cases} 12.92G_l & G_l \leq 0.0031308 \\ 1.055G_l^{\frac{1}{2.4}} - 0.055 & G_l > 0.0031308 \end{cases}, \\ B &= \begin{cases} 12.92B_l & B_l \leq 0.0031308 \\ 1.055B_l^{\frac{1}{2.4}} - 0.055 & B_l > 0.0031308 \end{cases}. \end{aligned} \tag{C.4}$$

If the XYZ tristimulus values were captured under a different illuminant, then a chromatic adaptation to the D65 illuminant. This can be performed using the following equations [20]:

$$\begin{aligned} \begin{bmatrix} X'' \\ Y'' \\ Z'' \end{bmatrix} &= \left[M_{CAT}\right]^{-1} \begin{bmatrix} \frac{R''_w}{R'_w} & 0 & 0 \\ 0 & \frac{G''_w}{G'_w} & 0 \\ 0 & 0 & \frac{B''_w}{B'_w} \end{bmatrix} \left[M_{CAT}\right] \begin{bmatrix} X' \\ Y' \\ Z' \end{bmatrix}, \\ \begin{bmatrix} R'_w \\ G'_w \\ B'_w \end{bmatrix} &= \begin{bmatrix} X'_w \\ Y'_w \\ Z'_w \end{bmatrix} \left[M_{CAT}\right], \begin{bmatrix} R''_w \\ G''_w \\ B''_w \end{bmatrix} = \begin{bmatrix} X''_w \\ Y''_w \\ Z''_w \end{bmatrix} \left[M_{CAT}\right], \end{aligned} \tag{C.5}$$

where X', Y' and Z' are tristimulus values under the captured illuminant and X'', Y'' and Z'' are tristimulus values under the target illuminant. Accordingly, X'_w, Y'_w and Z'_w are

tristimulus coordinates of the white point under the captured illuminant and X''_w, Y''_w and Z''_w are tristimulus coordinates of the white point under the target illuminant. The matrix M_{CAT} corresponds to a chromatic adaptation transform [20]. A common choice for this matrix is the Bradford transform [107]:

$$M_{CAT} = \begin{bmatrix} 0.8951 & 0.2664 & -0.1614 \\ -0.7502 & 1.7135 & 0.0367 \\ 0.0389 & -0.0685 & 1.0296 \end{bmatrix} \tag{C.6}$$

We remark that other chromatic adaptation transform matrices can also be chosen [20].

Index